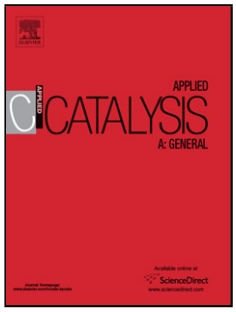

Title: Methane Dehydroaromatization over Molybdenum supported on Sulfated Zirconia Catalysts

Authors: Swarom Kanitkar, Md Ashraful Abedin, Srikar Bhattar, James J. Spivey

PII: S0926-860X(19)30032-8
DOI: https://doi.org/10.1016/j.apcata.2019.01.013
Reference: APCATA 16953

To appear in: *Applied Catalysis A: General*

Received date: 8 November 2018
Revised date: 16 January 2019
Accepted date: 20 January 2019

Please cite this article as: Kanitkar S, Abedin MA, Bhattar S, Spivey JJ, Methane Dehydroaromatization over Molybdenum supported on Sulfated Zirconia Catalysts, *Applied Catalysis A, General* (2019), https://doi.org/10.1016/j.apcata.2019.01.013

Methane Dehydroaromatization over Molybdenum supported on Sulfated Zirconia Catalysts

Swarom Kanitkar, Md Ashraful Abedin, Srikar Bhattar, James J. Spivey*

Cain Department of Chemical Engineering, Louisiana State University, Baton Rouge, LA – 70803, USA

*Corresponding author: J.J. Spivey, email: jjspivey@lsu.edu; Tel: +1-225-578-3690; Fax: +1-225-578-1476

Graphical abstract

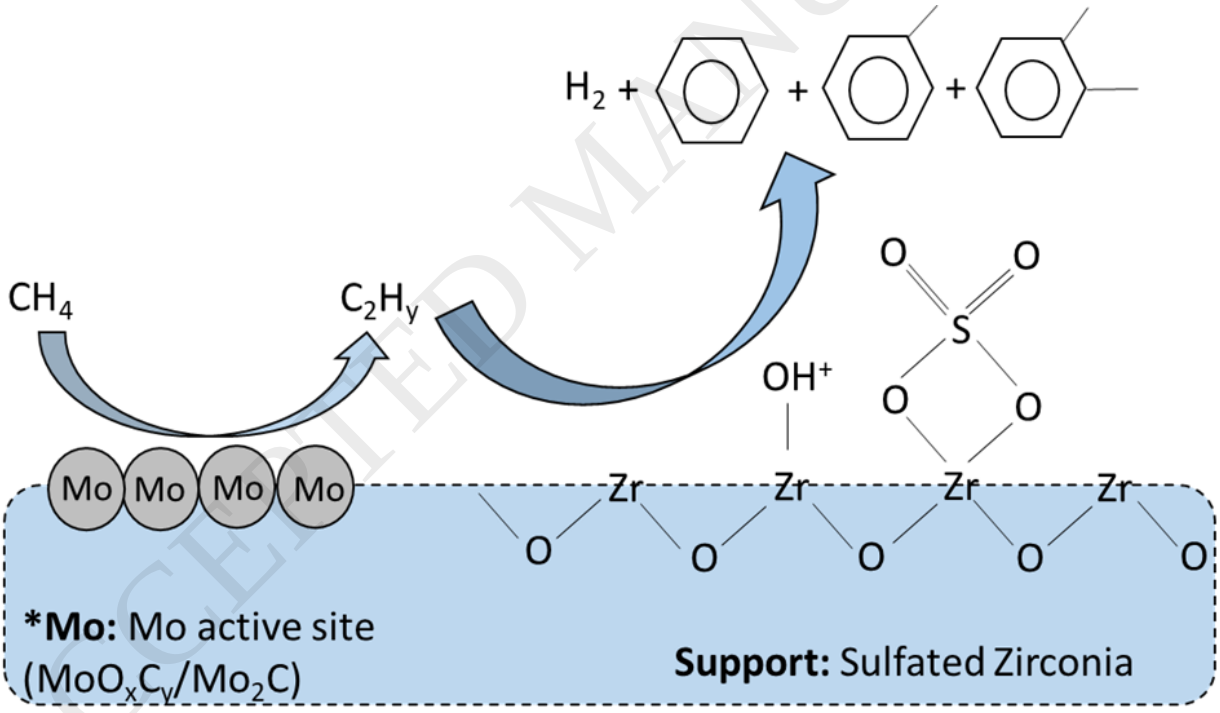

Highlights

- Sulfated Zirconia (SZ) is used as an acid support in CH_4 dehydroaromatization as compared to conventional H-ZSM-5
- Mo/SZ is characterized using XPS, XANES, and HRTEM

- Pyridine DRIFTS and NH_3-TPD confirms the presence and the nature of acid sites.
- Mo/SZ catalyst is more selective to heavier aromatics such as naphthalene as compared to Mo/H-ZSM-5 which is selective to lighter such as benzene
- Mo/SZ can be used in dehydrogenation, hydroconversion, or other light alkane aromatization reactions

Abstract

The shale gas revolution has strongly impacted the world by providing a significant incentive for research in natural gas conversion. Natural gas is becoming an important feedstock for the production of valuable chemicals. Dehydroaromatization (DHA) is an important non-oxidative conversion route for methane conversion, and Mo doped on the H-ZSM-5 or H-MCM-22 have been well-studied for this reaction. In these catalysts, Mo sites activate CH_4 to form dimeric species that are subsequently oligomerized on the strong Brønsted acid sites. In the present study, Mo is doped on solid sulfated zirconia (SZ) to create a catalyst similar to Mo/H-ZSM-5, but with a different solid acid. Despite the logic of using SZ as the acid, we are aware of no systematic study of Mo/SZ catalysts for this reaction. These catalysts were characterized using Raman, XPS, DRIFTS, SEM-EDS, HRTEM, XRD, XANES and other temperature programmed techniques. Raman spectra confirmed the formation of Mo=O and O-Mo-O bonds on the surface of SZ support. DRIFTS confirmed that there was little difference in acid sites when Mo was doped on SZ, except at higher Mo loadings. XPS, XANES, and HRTEM analysis showed that MoO_3 is converted to MoO_xC_y and is further converted to Mo_2C as the reaction progresses. Further, these catalysts were evaluated for methane DHA reaction. All of these catalysts showed methane conversions of 5-20 % at temperatures of 600-700 ^oC. In each case, the catalysts deactivated steadily, attributable to strong coking on the surface, as confirmed with TPO. A comparison with literature showed that Mo/SZ has comparable activity to Mo/H-ZSM-5 at around 650 ^oC - 675^oC temperature range. Further, Mo/SZ was more selective towards

heavier aromatics such as naphthalene and coke as compared to Mo/H-ZSM-5 at 700 ^{o}C, which is more selective towards benzene.

Keywords: Dehydroaromatization, Sulfated Zirconia, Natural Gas, Methane Conversion

Introduction

The conversion of methane into higher value chemicals is one of the grand challenges of 21st century. The shale gas revolution has made these immense, previously unattainable resources of natural gas accessible and economically competitive. Natural gas is considered to be a cleaner source than other conventional fuels such as coal and oil. This has helped some countries such as USA to reduce its CO_2 emissions by direct application of natural gas in the power plants [1, 2]. Conventional end-uses of natural gas include power generation or flaring, but it can also be used as a feedstock for the production of higher-value chemicals. Conversion of methane into higher-value chemicals has been long sought by researchers, but with limited success and generally with only incremental improvements.

The principal processes for conversion of methane can be categorized into non-oxidative or oxidative. Examples of oxidative route are as shown in **Figure**.

These include OCM (Oxidative Coupling of Methane) [3], Reforming (Dry/Bi/Oxy/Steam) [4-7], (PO) Partial Oxidation [8], Halogenation [9] or even Sulfidation [10]. Except for Steam Reforming of Methane (SRM) and Fisher Tropsch (FT), none of the other oxidative processes are commercialized and are often limited by the net yields of desired products. Though commercially practiced, SRM produces a syngas ($CO+H_2$) mixture, which is subsequently

converted into higher hydrocarbons, via processes such as Fisher Tropsch synthesis. Reforming processes produce commercially practical yields only at temperatures of 700-800 ^{o}C, which often results into high energy requirements and thus high costs [11]. On the contrary, non-oxidative conversion routes are based on a single step, thus requiring lesser energy and less cost. Some of the attempts involve use of what is known as superacids: HF-FSO_3H [12, 13], HF-SbF_5 [12, 13] or HBr-$AlBr_3$ [14] or sulfated zirconia (SZ) [15-17]. Other significant recent attempts involved use of lattice confined single Fe sites[18], use of metal modified zeolites (Mo [19, 20], Re [21], Ag [22], Zn [23]), or even recently using GaN nanowires under UV irradiation [24].

One of the potentially most important non-oxidative methane conversion processes is dehydroaromatization (DHA), the oligomerization of methane to benzene and hydrogen.

$$6\ CH_4 \leftrightarrow C_6H_6(g) + 9\ H_2 \uparrow \quad (\Delta G_{298K} = +433\ kJ/mol,\ \Delta H_{298K} = +530\ kJ/mol) \qquad (1)$$

DHA was first reported around 1966 in which methane was passed over silica gel at temperatures of around 1000 ^{o}C, with aromatic yields of 4-6 % [25]. It was not until 1990s that DHA attracted attention [19, 20]. Molecular sieves such as H-ZSM-5 zeolite and H-MCM-22 have been shown to be the most active supports for this reaction [26-28]. Many reports based on doping of noble metals such as Mo, Re, or W into these supports for the aromatization of methane have also been reported [29]. Nevertheless, the literature shows that Mo-doped catalysts have been the most widely-studied catalysts for DHA. Despite a great deal of research, and significant improvements to the process, e.g., using membranes to separate hydrogen, DHA has not yet been commercialized.[30-32]

It is widely accepted that active molybdenum oxycarbide or carbide species are generated in-situ under reducing reaction conditions and under the flow of methane [26, 27]. These species

can also be intentionally generated using other carbon sources (CO_2/CO) under H_2 flow [26, 27]. Even though the nature of active species oxycarbidic/carbidic is not fully understood [29], it is commonly believed that exchanged molybdenum [33] species activate methane by activating one of the C-H bonds that lead to the formation of CH_x species, forming a dimer: C_2H_y. This dimer is then oligomerized and cyclized into higher hydrocarbons and aromatics on the Brønsted acid sites (BAS) of the molecular sieve. This mechanism has been opened for debate as to whether it is bifunctional or monofunctional, based on one study [34]. Regardless, this typical bifunctional mechanism can be depicted as shown in equation 2 (BAS=Brønsted acid site) [26]:

$$CH_4 \overset{\text{Mo site}}{\longleftrightarrow} C_2H_y \overset{\text{BAS}}{\longleftrightarrow} C_6H_6 + C_7H_8 + C_8H_{10} + H_2 \quad (2)$$

There are a number of solid acids that could, in principle, catalyze the C_2H_y species. For example, sulfated zirconia (SZ) is a well-known solid superacid that has been studied and a number of variations have been produced (mesoporous, nanosized, e.g.) [35-37]. SZ possesses strong BAS that can play a key role in the oligomerization of dimeric species. In principle, a similar bifunctional catalyst could be synthesized if Mo is doped onto a solid acid. Although doping of Mo on SZ is not novel [38]; to the best of our knowledge, no study has shown DHA of methane on these catalysts.

The present work tests these Mo/SZ catalysts for DHA of methane and also the effect of Mo loading at reaction conditions of interest. For this purpose, 3 different catalysts were synthesized: SZ (w/o Mo), and two Mo loaded SZ catalysts with two different loadings of Mo (1 %, 5 %). These catalysts were further evaluated for DHA and were characterized using spectroscopic techniques including Raman, DRIFTS, XRD, SEM-EDS, XANES, HRTEM, XPS. The hypothesis is that an active DHA catalyst can be prepared based on Mo/SZ, incorporating the requisite metal and acid sites for this reaction.

Experimental

Materials

Zirconium hydroxide, $Zr(OH)_4$ (97 %) and ammonium molybdate tetrahydrate $(NH_4)_6Mo_7O_{24}.4H_2O$ were both purchased from Sigma Aldrich Inc. H_2SO_4 (95 – 98.0 %) was purchased from Malinckrodt Chemicals Inc. Ultra-high purity grade H_2, CH_4, Ar, and 10% O_2/He were all purchased from Airgas Inc. NH_4-ZSM-5 (Si/Al = 50:1) was purchased from Alfa Aesar Inc. All Mo standards (Mo powder, MoS_2, MoO_3, MoO_2, β-Mo_2C) were purchased from Alfa Aesar Inc. with a purity of 99+%.

Catalyst Preparation

Sulfated zirconia was prepared based on literature methods [36]. In a typical preparation, about 35 g of $Zr(OH)_4$ was mixed with 500ml of 0.5 M H_2SO_4 solution and the mixture was stirred for 2 hr, followed by vacuum filtration and subsequently dried overnight at 110 ^oC. The dried catalyst powder was then calcined at 550 ^oC for 4 hrs under static air to get the sulfated zirconia catalyst. Different loading of molybdenum were incorporated onto sulfated zirconia using standard impregnation method. In a typical preparation, known quantity of ammonium molybdate tetrahydrate was dissolved in 50 ml of water and to this solution, appropriate quantity of sulfated zirconia was added and the solution was stirred for 2 hours after which a similar procedure of vacuum filtration, overnight drying (110 ^oC) and calcination at 550 ^oC for 4 hrs in static air was followed. This yielded the final Mo supported on sulfated zirconia catalysts. Similar procedure was also used for preparing Mo supported on H-ZSM-5 catalysts. For H-ZSM-5 preparation, as purchased NH_4-ZSM-5 was calcined at 550 ^oC for 4 hrs under static air.

ICP-OES

Inductively coupled plasma – optical emission spectroscopy (ICP-OES) was carried out using Varian-MPX spectrophotometer in Wetland Biogeochemical Lab at LSU Oceanography. The digestions of samples were carried out using a mixture of borate flux: Lithium Tetraborate (49.75

wt%), Lithium Metaborate (49.75 wt%), and Lithium Iodide (0.5 wt%). In a typical procedure, 0.2 g of catalyst sample was mixed with 2 g of borate flux mixture. This mixture was fused in a furnace at 1000 ^{o}C and subsequently dissolved in a warm 10% HNO_3 solution. This solution was diluted subsequently and used for ICP-OES analysis.

BET

Breauner Emmett Teller (BET) surface area analysis was done using Altamira AMI-200 catalyst characterization system using N_2 monolayer adsorption. Three-point BET with 10 %, 20 % and 30 % N_2 concentrations in Helium was used to estimate the surface areas of these catalysts.

Raman Spectroscopy

Analysis by Raman spectroscopy for all catalyst samples was carried out using Renishaw inVia Raman microscope equipped with 532 nm (green) laser was used. Spectra measurements were carried out at 10 mW power and with 50 µm slit aperture.

DRIFTS

Diffuse Reflectance Infrared Fourier Transform Spectroscopy (DRIFTS) experiment using pyridine as a probe molecule was carried out in a Thermo Scientific Nicolet 6700 FTIR equipped with Harrick Praying Mantis reaction cell fitted with KBr windows. Spectra of all the samples were recorded with a spectral resolution of 4 cm^{-1} in region going from 4000 – 650 cm^{-1}. In a typical experiment, IR cell was loaded with the catalyst sample inside the glovebox. Sample was then brought on stream and pretreated at 100 °C for 30 minutes under He flow to clean the surface of the catalyst from adsorbed impurities. After pretreatment, sample was cooled down to 25 °C and a background spectrum was recorded. At this temperature, catalyst was saturated with pyridine vapors for 3 hrs. Saturated sample was then treated under He flow for 30 minutes to remove physisorbed pyridine from the catalyst surface and from the cell chamber. Sample was then treated at 100 ^{o}C for 10 minutes under He flow and cooled back to room temperature

and the actual spectrum was recorded. Similar spectra were recorded at room temperature after 10 min. treatments at 200 °C, 300 °C, and 400 °C to check the thermal stability of the acid sites on catalysts.

Ammonia-TPD

Ammonia-TPD was carried out using Altamira AMI-200 reactor system in conjunction with Ametek Mass Spectrometer. Typically 50 mg of catalyst was weighed and loaded in a quartz tube reactor. Catalyst was pretreated at 100 °C for 30 min under He flow to clean the catalyst surface. After pretreatment, sample was cooled down to 50 °C, and ammonia was adsorbed by flowing it through the catalyst bed for 1 hr. Post ammonia adsorption, 25 sccm of He was flown for 40 min to remove any physisorbed/residual ammonia. At this time, Mass Spectrometer and TCD detector were turned on and the temperature was ramped up at 10 °C/min. from 50 °C to 500 °C.

The TCD signal is usually a combination of signals from various gases that are generated or are being flowed in the system. In order to clearly distinguish various gases coming out, MS was used to track signals for following masses: 4, 16, 17, 18, 27, 32, and 82. Based on ammonia (m/e =16) signals from MS with respect to temperature, amounts of ammonia desorbed and peak positions were calculated.

SEM-EDS

SEM analysis of the samples was done at LSU Shared Instrument Facilities (SIF) using FEI quanta 3D FIB/SEM equipped with Ametek EDAX accessory. Samples were analyzed at a voltage of 5 kV and at a resolution of 3 µm.

HRTEM

High Resolution Transmission Electron Microscope (HRTEM) was used to study these type of catalysts. This was particularly useful in confirming the loading of Mo onto the sulfated zirconia

sample and also to confirm the formation of Mo_2C after carburization of the fresh catalysts was done. HRTEM scans of these catalysts were obtained using JEOL JEM-2011 Scanning TEM at an accelerating voltage of 200 kV.

XRD measurements

XRD measurements for all the samples was carried out using PANAnalytical EMPYREAN diffractometer with Cu K_α radiation. Sample was collected by scanning the data from 5^o to 90^o with a step size of 0.026 sec/pt. Data analysis of XRD of all samples was done using PANAnalytical X'Pert software.

XPS

X-ray Photoelectron Spectroscopy for the samples was performed at Shared Instruments Facility (SIF) in LSU. All the analyses were performed on Scienta Omicron ESCA 2SR instrument with Mg as an X-ray source at 15 kV and at a pass energy of 40. Post processing of XPS data was performed using CasaXPS software.

XANES

X-ray Absorption Near Edge Spectroscopic (XANES) studies of the catalyst were performed at the electron storage ring of J. Bennett Johnston, Sr., Center for Advanced Microstructures and Devices (CAMD) of Louisiana State University, Baton Rouge, Louisiana. CAMD operates the ring operating at 1.3 GeV with current between 100 mA to 50 mA. The Mo K edge measurements were made at the High Energy X-ray Spectroscopy (Hexas) beamline located on an 11-pole wiggler operating at 5.5 Tesla. The L_{III} edge measurements were made at the Low Energy X-ray Absorption Spectroscopy (Lexas) beamline, a windowless beamline on a bending magnet with a 13 µm Kapton tape separating the ring from the beamline. Both beamlines use Lemonnier double crystal monochromator with design modifications made at the University of

Bonn. At lower energy InSb 111 crystals (resolution ca. 0.5 eV) were used while at higher energy water-cooled Ge 422 crystals (resolution ca. 2 eV) were used.

For Mo K edge measurement, the Hexas beamline was calibrated with a Mo Foil at 20 keV. The beamline has three ion chambers with a Mo foil in between the second and third chambers for monitoring the calibration. Mixtures of argon, and xenon gases were used to achieve 20%, 30% and 30% absorption in the first, second and third chamber, respectively.

Mo standards used in the analysis were: MoO_3 (99.9% metals basis, Alfa Aesar), Mo foil (−200 mesh, 99.9% metals basis, Alfa Aesar), and Mo_2C (99.9% metals basis, Alfa Aesar). The standards were measured in transmission while the catalyst samples were placed on Kapton tape and scanned in fluorescence using a seven-element Ketek silicon drift detector with a total area of 560 mm^2 and a resolution of ca. 135 eV.

The low energy beamline was calibrated with the zinc sulfate white being at 2481.44 eV. The ion chambers used air as ionizing gas, the chamber being evacuated to 50 Torr. A single-element Ketek silicon drift detector with an active area of 150 mm^2 was used for fluorescence signal detection.

Carburization and Dehydroaromatization (DHA)

MoO_xC_y or Mo_2C, which are the active species for DHA reaction were generated in-situ. For this, a procedure from the literature [38] was followed. First, Mo catalyst (oxidized form) was reduced under H_2 at 10 K/min ramp rate from room temperature to 650 ^oC. After 650 ^oC temperature was reached, CH_4 gas was introduced into the reaction system for 4 hrs at a ratio of 1:4 (CH_4:H_2). This treatment led to carburization of the MoO_x species. After 4 hours, hydrogen and methane was turned off and the system was purged with argon. Subsequently pure CH_4 was introduced at the desired reaction temperature to carry out DHA reaction. All of these sequences were carried out in an Altamira AMI 200HP reactor system equipped with a SGE

glass lined SS tube. In a typical experiment, reactor tube would be loaded with (0.3 – 1) g of carburized catalyst and small quantities of CH_4 (10 sccm) and Argon (5 sccm, internal standard) would be passed over the catalyst bed. Reaction products were analyzed downstream using Shimadzu GC2014 (FID, 2 TCD's) equipped with Restek RT-Q-Bond column (30 m x 0.53 mm x 20 μm) in conjunction with Shimadzu QP2010 GC-MS system. We would like to point out that we were not able to measure Naphthalene in our GC system. Also, estimating coke content at any point during reaction is a challenge. So, based on the products observed and the amount of methane converted, we estimated combined naphthalene and coke content at any time on stream.

Following formulas were used for the activity calculation:

$$\% \ CH_4 \text{ conversion} = \frac{\text{conc. } CH_{4_{in}} - \text{conc. } CH_{4_{out}}}{\text{conc. } CH_{4_{in}}} \times 100$$

Selectivities were calculated based on observable products and naphthalene and coke content was estimated based on the amount of methane converted.

$$\%C \text{ selectivity} = \frac{\text{carbon number in the product} \times \text{conc. Product}}{\text{conc. } CH_4 \text{ reacted}} \times 100$$

Results and Discussion

Physico-chemical properties of the catalyst

Physical and chemical properties of the catalysts are listed in **Table 1**. Base SZ catalysts in the literature are reported to have surface areas of 50-100 m^2/g [39]. The present SZ catalyst has a surface area of 84 m^2/g, well within the expected value. As the Mo was doped onto SZ, it lead to slight decrease in the surface area, as expected, due to blockage of pores as expected from the loading of Mo [38, 40]. However, in the case of 1% doping of Mo, there is no statistical difference between the BET surface areas.

Table 1 shows the elemental Mo loading to be 0.84 and 3.92 wt% as compared to intended 1 and 5 wt% loading. We believe that it is quite possible that some of the Mo was lost during vacuum filtration while synthesis of the catalysts.

S (sulfur) loading from ICP also is shown in **Table 1**. It shows that the base SZ had sulfur content of 3.5 wt%, which was reduced as Mo was doped into this catalyst. This decrease was proportional to amount of Mo loaded. When 1wt% Mo was loaded, it decreased slightly from 3.5 to 2.99 and further to 1.95 wt% when, 5 wt% Mo was loaded. This is quite possible because when Mo is impregnated onto this catalyst and interacts with or replaces the SO_4^{2-} species on the surface. This could be seen subsequently in Raman spectroscopy as well.

Raman spectroscopy

Raman spectroscopy is used to detect non-IR specific bond vibrations and can be useful to analyze inorganic compounds which are not IR-active. **Figure** shows Raman spectra for a sulfated zirconia as a base sample (a) and a transition of 5% Mo/SZ catalyst from oxidized form (b) to a carburized one (c), and to a spent one (d).

Common bands observed for sulfated zirconia include ~ 270 cm^{-1}, ~ 320 cm^{-1}, ~ 460 cm^{-1}, ~ 650 cm^{-1} and 1025 cm^{-1}. These bands below 700 cm^{-1} are attributed to tetragonal ZrO_2 vibrations [36], while the band at 1025 cm^{-1} is attributed to vibrations from sulfate groups on ZrO_2 surface. When Mo was introduced into this catalyst, two distinct new bands appear around ~ 820 cm^{-1} and ~ 970 cm^{-1} Raman shifts (shown in the box in Figure 2). These bands are attributed to the Mo-O-Mo, and Mo=O vibrations [41] respectively. This confirms doping of Mo on the surface of sulfated zirconia.

An attempt to measure the Raman spectra for spent catalyst samples, or even for a carburized fresh catalyst, was difficult because these samples were grey/dark, causing a strong absorption of the energy from the excitation source [42]. Similar difficulties were also experienced by the same authors [42] in obtaining FTIR spectra for carburized MoO_3 samples. Despite of this, we

made an attempt to focus on a different spot location and this provided a meaningful spectra for these samples. Moving from (b) to (c) and to (d), i.e. from an oxidized catalyst to a spent catalyst, most of the bands corresponding to t-ZrO_2 show very little difference. Also, band corresponding to Mo-O-Mo vibration (~ 820 cm^{-1}) appears to be normal but the band corresponding to Mo=O vibration (~ 970 cm^{-1}) appears to have shifted higher (~ 995 cm^{-1}). This shift might indicate the presence of a carbidic form of molybdenum [38]. In addition to these differences, there are two new bands at 1340 cm^{-1} and 1600 cm^{-1} in the case of carburized and spent samples, which may be attributed to the D and G bands of graphitic carbon [43, 44]. As expected, these bands were intense for the spent sample than the carburized one, indicative of more carbon deposited on the surface.

Another noticeable change between these samples is the loss of intensity for the band at ~ 1025 cm^{-1} corresponding to the sulfate groups, which may be due to the interaction between Mo and SO_4^{2-} groups during the impregnation process and also probably due to volatility of SO_4^{2-} species during the carburization and the reaction [38].

DRIFTS

DRIFTS in conjunction with pyridine as a probe molecule was used to characterize the acid sites of the catalyst. Base SZ catalyst is known to have both Brønsted and Lewis strong acid sites [16, 17, 36]. This was confirmed by observing the shift in vibrations from adsorbed pyridine at ~ 1445, 1610 cm^{-1} (co-ordinated pyridine), and ~ 1540 cm^{-1}, 1640 cm^{-1} (protonated pyridine) that are present in all the samples [45]. Bands at ~ 1490 cm^{-1} correspond to pyridine adsorbed on both Lewis and Brønsted sites [45, 46].

A comparison of DRIFTS spectra for catalysts with different loadings of Mo is presented in **Figure**. When Mo was doped in different amounts on the base SZ catalyst, the type of acid sites did not change. Both Brønsted and Lewis acid sites were still present and there was little

qualitative difference in the concentration of acid sites. However, as the loading of the Mo increased, bands corresponding to both types of acid sites shifted slightly towards lower wavenumbers. This indicates a slight decrease in the strength of the acidic sites, possibly due to interaction of Mo oxides with the hydroxyl groups and oxygens on the surface of SZ [47]. Also, a qualitative slight increase in the concentration of Lewis acid sites could be seen. This could have been due to generation of MoO_3 species that are Lewis acidic in nature [47, 48].

The thermal stability of acid sites up to 400 ^oC was tested [shown in Supplementary Information (SI), 2.2]. Despite higher temperatures, all the catalysts maintained both types of acid sites and the pattern was quite similar for all.

NH_3-TPD

Ammonia TPD of all the catalysts showed strong acid sites. TPD results for Mo-doped catalysts followed a trend similar to that of base SZ catalyst. Several reports [36, 37, 46] suggest that beyond 600 – 700 ^oC, sulfates on the surface start to decompose (considering that the calcination temperature was 550 ^oC). This often generates a false signal in the TCD, but this signal can be correctly distinguished from the ammonia signal using a mass spectrometer as was done in the present case. A signal corresponding to (m/e = 32) started to appear beyond 630 ^oC, confirming the decomposition of sulfate species [46].

Figure 1 shows a comparison of NH_3-TPD curves for all four different catalysts: base SZ, and three Mo doped SZ catalysts (1%, and 5% doping). Sulfated zirconia typically has a desorption peak at around 160 ^oC and a long shoulder that decreases slowly down to ~ 550 ^oC. As Mo was doped in increasing concentrations onto SZ, the low-temperature peaks (~160 ^oC) are essentially the same as that of SZ alone. The shapes of the TPD are remarkably similar, for lower Mo content, suggesting that the acidity is due to SZ alone. At higher loading, shapes of the curve slightly change indicating a reduction in acid sites. The total acidity, as measured by

TPD, also decreases with loading. There are several explanations: one is that the high loading may cover the catalyst surface sufficiently to affect access to the acidic sites. Another is that the interaction between Mo and SO_4^{2-}, as pointed out earlier. Finally, another could be the addition of Lewis acidic MoO_3 species on the surface that may counteract the earlier and the net result is what we see (increase in acidity through Lewis acidic MoO_3 and decrease in acidity due to possible replacement of some of the SO_4^{2-} groups by Mo).

Figure 1: NH_3-TPD comparison for all the catalysts (a) SZ, (b) 1% Mo/SZ, and (c) 5% Mo/SZ. Values next to each curve represent quantity of NH_3 desorbed per gram of catalyst

XPS

Figure shows Mo 3d XPS spectra for 8 different catalysts, including 5 standards along with 3 samples of the most active catalyst (5% Mo/SZ) after various treatments. The first one (a) is MoO_3 standard (thermodynamically most stable oxide of Mo), which shows standard 3d spin orbit coupling of $3d_{5/2}$ (BE = 233 eV) and $3d_{3/2}$,corresponding to a +6 oxidation state [49]. Sample (b) shows the fresh catalyst (oxidized form) without any treatment. This sample very closely resembles with that of (a), indicating the presence of MoO_3 on the fresh sample. The third sample (c) is the fresh (oxidized form) carburized for 4 hrs under a flow of CH_4:H_2 at a ratio of (1:4) at 650 ^oC after reduction under H_2. This sample shows peaks corresponding to MoO_3 and another third peak at BE ~ 229 eV. This peak likely corresponds to oxy-carbide phase of Mo (MoO_xC_y).

The fourth sample (d) is the spent catalyst sample after running the carburized sample in the CH_4 aromatization reaction at 650 ^oC for 1000 min on stream. This sample also shows three peaks with two resembling MoO_3 and the third one slightly shifted towards right (BE ~ 228.6 eV) as compared to carburized form. This more closely resembles the Mo_2C phase. In order to verify this, standards directly purchased from the manufacturer were tested: β-Mo_2C (e), MoO_2 (f), MoS_2 (g), Mo powder (h). Mo_2C standard shows peaks corresponding to oxide phase and a

small third peak at BE ~ 228.4 eV. MoO_2 is another form of Mo oxide which clearly shows three peaks: two corresponding to MoO_3, however, the third one corresponds to +4 oxidation state ($3d_{5/2}$) [50]. Since the catalysts of interest here involve Mo and S and especially Mo '3d' and S '2s' regions overlap, so to remove any doubt about formation of MoS_2 or overlapping issues, the MoS_2 sample (g) was tested. It shows two large peaks that correspond to 3d5/2 and 3d3/2 of Mo corresponding to +4 oxidation state [51] and a small peak at ~226 eV, corresponding to S '2s'. Clearly, MoS_2 contains substantial amount of sulfur and still S '2s' peak is weak. Thus, in the samples of interest (Mo/SZ), S content being very small compared to the 'S' content from MoS_2, we expect negligible influence due to S '2s' peak and the peaks we observed correspond only to Mo 3d. Finally, the Mo powder standard (h) would be expected to be in reduced form, Mo (0). For this standard, we saw three peaks, two corresponding to Mo (+6), one shoulder that might correspond to some intermediate oxide phase (+5), and a small peak at ~ 228.2 eV, which most likely corresponds to the reduced Mo (0) [50]. On the basis of these observations, the carburized sample is initially in the oxycarbide phase, then subsequently transformed into Mo_2C under reaction conditions.

Note that the samples were not run in-situ, so it is possible that part of the samples was oxidized due to exposure to room conditions, forming peaks corresponding to these oxidized parts of the catalyst, even in standards such as Mo_2C, Mo powder, or MoO_2, which show peaks corresponding to MoO_3.

XANES

Mo K-edge (**Figure**) and L_{III}-edge XANES (shown in SI, 2.5) spectra provided the evidence for the formation of Mo_2C or MoO_xC_y phases, which are generally believed to be the active sites for methane conversion. **Figure** shows K-edge XANES spectra for various Mo catalyst samples along with two reference samples of MoO_3 and Mo_2C. Spectra for MoO_3, fresh catalyst (oxidized form), and carburized show a pre-edge feature that indicates the oxidation state of +6 and is

attributable to the quadrupole/dipole transition from 1s to 4d orbital [33]. After the pre-edge region, the edge region indicates a sharp jump in the energy of absorption edge corresponding to 1s to 5p dipole transition.

Spectra for the fresh catalyst sample resembles MoO_3 closely with a similar pre-edge feature that is commonly observed in the case of Mo/H-ZSM-5 catalysts [33, 52, 53].
For the carburized, and the spent sample, there is a reduction in the energy of absorption edge, indicating the reduced state of Mo in both these samples (carburized and spent). This reduction in edge energy from fresh (oxidized form) to spent (after reaction) was around ~ 7 eV that corresponds well within the literature [33, 52]. Mo_2C reference and the spent catalyst sample have similar absorption edge energies. Also, for the carburized and the spent sample, the pre-edge peak disappears. This disappearance is apparent as pointed out by the arrow in **Figure**. Since the absorption edge energies for carburized and spent catalysts are higher than Mo_2C, it provides evidence for the existence of more oxidized species than Mo_2C (Mo, +2), such as MoO_xC_y that disappear as the reaction progresses and spent catalyst closely resembles Mo_2C [52, 53].

Figure shows that the reference samples: MoO_3 and Mo_2C have stronger oscillations in the EXAFS region farther from the edge. However, 5% Mo/SZ samples with different treatments (fresh, carburization, and reaction) do not have these oscillations in the EXAFS region. This might be an indication that the well dispersed Mo species in the SZ matrix are without any long range order [33].

HRTEM

HRTEM was performed on all of the catalysts but the results for the 5% Mo/SZ are shown here since it has the highest activity (reaction data section). Four different images are shown for four different phases: SZ, 5% Mo/SZ (fresh - oxide form), 5% Mo/SZ (carburized form), and 5%

Mo/SZ (spent form). All these images also have SADP (selected area diffraction pattern) images in the inset.

There are two phases of ZrO_2 in XRD (shown in SI, 2.4), monoclinic (m) and tetragonal (t), and tetragonal being the primary phase. In HRTEM analysis, primarily monoclinic (m-ZrO_2) planes (111) were observed with few t-ZrO_2 (011). **Figure** shows an image for the base SZ. Planes corresponding to planes of m-ZrO_2 and t-ZrO_2 are seen. However, a bulk analysis of a sample shows rings corresponding to t-ZrO_2 (011, 002, 020, 121, etc.) as shown in the inset of **Figure**. This illustrates the SADP for a zoomed-out sample. This confirms the observations from XRD (shown in SI, 2.4) that the bulk phase of ZrO_2 was tetragonal.

When Mo was impregnated on SZ, new planes appear, corresponding to MoO_3 species, as seen in **Figure**. Further, Mo appears finely dispersed in the SZ matrix [54, 55] as seen in **Figure**. Tetragonal zirconia (t-ZrO_2) was also detected that often is the crystalline part of sulfated zirconia as detected in XRD [36].

For the carburized catalyst, in addition to ZrO_2 planes, other planes were observed. Some of these planes correspond to MoO_3. There are also planes that correspond to Mo_2C and there are some that do not belong to either MoO_3 or Mo_2C, along with ZrO_2. This could be due to the formation of an intermediate phase of MoO_xC_y [56, 57]. Formation of Mo_2C was also confirmed using HRTEM of carburized sample of 5%Mo loaded on SZ catalyst, as observed in **Figure**. A small portion on the carburized sample showed d spacing corresponding to (111, 201) plane of Mo_2C.

When this carburized sample is run further under DHA conditions for 16 hrs, there are changes in the lattice planes. **Figure** shows HRTEM of a spent 5% Mo/SZ catalyst sample. Greater amounts of carbon were observed and this carbon can be divided into two types: graphitic (primarily around the edges) and amorphous (over the entire sample). There are also 2 – 3 nm

particles around the edges, which most likely correspond to Mo_2C nanoparticles [54]. Surrounding these particles, there are few layers of graphitic carbon. Similar results can be observed in the literature [54, 55, 58, 59], which confirmed the presence of Mo_2C in H-ZSM-5.

These results show that Mo is finely dispersed in SZ matrix and it also shows the state of Molybdenum through different phases of reaction and treatments: Fresh -> Carburized -> Spent. TEM analysis confirmed the conclusions drawn from other characterizations and explains this Mo transition from oxidized form into the oxycarbide form and finally into the carbidic form. TEM also supported the observations from XRD (shown in SI, 2.4) about the bulk phases of the sample.

Reaction Data

Effect of Mo content

Results of reaction runs from the Mo-doped SZ catalysts varied considerably (**Figs 11 and 12**) albeit majority of the runs had naphthalene and coke as primary products. Among other products included ethylene, ethane, propylene, propane, and aromatics including benzene, toluene and xylenes along with hydrogen. There are several general trends of conversion and selectivity as a function of Mo loading and time. First, methane conversion decreases with time at all Mo loadings. This can be attributed to coke formation, which likely forms almost initially and accumulates with time-on-stream. Second, selectivity to aromatics is generally ~ 10-15 % initially, but decreases rapidly with time. These compounds are believed to be the precursors for polynuclear aromatic compounds, which comprise coke.

The rate at which methane conversion decreased varied slightly from catalyst to catalyst, depending on Mo loading. The 1% Mo/SZ showed a rapid drop in conversion of methane as compared to 5% Mo/SZ. For the 1% Mo/SZ catalyst, the conversion dropped from ~ 14 % to ~ 5% in 16 hours. However, 5% Mo loaded catalyst showed more gradual decrease in the

conversion of methane, from ~ 20 % to 6.5%. For the 5% Mo/SZ catalyst, even the selectivity to non-coke products for this catalyst did not show a rapid drop as compared to the 1% Mo/SZ. Overall, 5% Mo loaded catalyst showed higher overall conversion compared to the other catalyst.

Ethylene selectivity is a clear anomaly. For both catalysts, ethylene selectivity generally increased with time up to ~ 10-12%. For the 1% Mo/SZ catalyst, ethylene selectivity does not significantly decrease with time after 600-700 min, even when methane conversion decreases. For the 5% Mo/SZ catalyst, there is some decrease in ethylene selectivity after 600-700 min. It is clear that the dimerization of methane is a primary product of methane conversion on both catalysts, and subsequent conversion to measurable products is relatively less selective. This supports the general observation that active Mo sites are responsible for the production of C_2 dimers. Higher loadings of Mo contain more active sites, but these sites are of comparable selectivity. Over time, coke deposition starts to block the BAS, decreasing the rate of formation of aromatics and blocking access to the Mo active sites, though selectivity to ethylene is relatively steady beyond ~700 min on stream. These results indicate that the coke deactivates BAS first and subsequently deactivates Mo active sites. Similar results have been observed in the literature [60] in which it was found that the rate of formation of C_2-C_3 hydrocarbons increased with decreasing benzene and naphthalene selectivity rates. The large amount of naphthalene and coke is likely due to high rates of cyclization and dimerization of olefinic C_2 intermediates over strong acid sites from sulfated zirconia.

Selectivity to higher aromatics such as ethylbenzene or xylenes (o, m, p) increased over time (not shown) but was negligible. During an initial period of several hours, there was no measurable formation of these compounds. Only benzene and toluene could be observed during these initial hours. As the methane conversion decreased, the formation of these higher aromatics increased. This trend was true for both the catalysts.

Coke deposition is the most probable reason for deactivation of these catalysts, although loss of SO_4^{2-} groups (SI, 3.2) from the surface of sulfated zirconia at high temperatures could also be responsible for deactivation [46]. This loss could not be ruled out because during NH_3-TPD, starting at around 620^{o}C, the oxygen signal (m/z = 32) was detected, indicative of an oxide compound decomposition. ZrO_2 being very stable compound (m.p. = 2715 ^{o}C), it is unlikely that Zr-O bonds would break down. Neither would any molybdenum oxide based compound because MoO_3 sublimes at ~ 1150 ^{o}C. The only remaining source of oxygen then could be from SO_4^{2-} groups, which are co-ordinated on the surface of ZrO_2. Similar decomposition of sulfated ZrO_2 has been observed in the literature [61], indicating that O_2 from the ZrO_2 structure is highly unlikely, so the oxygen from SO_4^{-2} could be responsible for that signal.

Effect of temperature

Since 5% Mo doped SZ activity/selectivity was representative of the other catalysts, the effect of reaction temperature was studied using this catalyst. Methane DHA has been typically studied in the temperature range of around 700 ^{o}C [27]. Sulfated zirconia is not stable beyond 700 ^{o}C, and starts to decompose at ~ 620 ^{o}C [62]. Thus, the effect of temperature on 5% Mo doped SZ was studied at 600, 650, and 700 ^{o}C, spanning this temperature range of interest here.

Table 2 shows that methane conversion increased with temperature, reaching ~ 20 % at 700 ^{o}C. The aliphatic and aromatic selectivities show no clear trend with temperature. The results in **Figs. 13, and 14** are the net result of competing rates of reaction, deactivation, and the rate of sulfate decomposition from surface. The reaction rate increases with temperature while deactivation due to sulfate decomposition is more rapid as well. This has been observed on Mo/H-ZSM-5 catalysts as well [27, 63], in which higher temperatures led to higher activity but faster deactivation because rate of naphthalene and coke formation also increases. This is apparent for Mo/SZ catalysts as seen in **Table 2** as well. **Figure** shows that ethylene increases monotonically with time, reaching ~8 - 9 % selectivity at higher temperatures, then decreases.

Selectivity goes through a maximum. In the case of higher temperatures, selectivity drops quickly. Activity decreases more rapidly at higher temperatures. This might be due to a faster rate of deactivation at higher temperatures. Except for lower temperature of 600 ^{o}C, selectivity continues to increase with time on stream.

Benzene selectivity also goes through a maximum and then decreases constantly with time at each temperature (**Figure**). A rise in ethylene selectivity and a drop in benzene selectivity suggests that the sites for conversion of the dimers to benzene are deactivated by coke deposition with time, and this trend is seen at all three temperatures tested here. But this does not mean that there is no deposition of coke on methane activation sites. Note that methane conversion is decreasing as well, so that the yield of ethylene is decreasing despite the fact that the selectivity is increasing. This indicates that coke is deposited on Mo sites as well, as shown by HRTEM that graphitic carbon layers around Mo particles (see **Fig. 11**).
The main difference for the lower benzene selectivity at 650 ^{o}C and 700 ^{o}C, as compared to 600 ^{o}C, might be due to loss of BAS through loss of volatile SO_4^{2-}.

Similar conclusions can also be drawn from TPO (SI 3.1, Fig. S11) ran for these three spent catalyst samples. Catalyst ran at 700 ^{o}C showed highest amount of coke deposited only to be followed by catalyst ran at 650 ^{o}C and the least amount of coke was observed on the catalyst ran at 600 ^{o}C.

Effect of space velocity

Figures 15, 16, and 17 show that higher space velocities over 5% Mo/SZ lead to both lower CH_4 conversion (**Fig. 15**), and to lower benzene selectivity (**Fig. 17**). This is expected because often this reaction is not considered as mass transfer limited [63]. **Figu re *16*** shows that ethylene selectivity initially increases slowly, corresponding to high initial benzene production (**Fig. 17**). However, this changes very quickly with time-on-stream as ethylene selectivity goes

through a maximum whereas, benzene selectivity decreases rapidly. This can be attributed to coke formation, which blocks BAS and limiting the aromatization of ethylene. Ethylene selectivity reaches a similar steady state in all three SVs (**Figu re *16***), but the maximum is reached at earlier times-on-stream as the space velocity is increased. The maxima in ethylene selectivity represents the result of two rates: ethylene formation from methane, and ethylene reaction leading to benzene. With time, benzene selectivities decrease to near-zero values, while ethylene selectivities reach a steady state. This means that although very little benzene is formed after ~1000 min, active sites capable of reacting ethylene to products reach a quasi-steady state at the same SVs, at least at the times investigated here. Coking leads to blockage of BAS that in turn affects the production of benzene. Mo sites are also blocked but possibly at a slower rate than BAS. Thus, selectivity to ethylene reaches a steady state value although the methane conversion is still decreasing.

TPO (SI 3.1, Fig. S12) results on the spent catalysts showed that the greatest coke deposition was observed on the lowest space velocity of 0.6 $Lgcat^{-1}hr^{-1}$, while the lowest coke deposition was found on the catalyst ran at highest space velocity of 1.8 $Lgcat^{-1}hr^{-1}$. This was surprising because the rate of decay in benzene formation (Fig. 17) and time to reach maximum ethylene selectivity (Fig.16) was faster in the case of higher space velocity, whereas the amounts of coke at those space velocities were lower. This can be attributed to the preferential nature of coke formation near outer surface of catalyst particles [63, 64]. Additionally, in these type of reactions benzene production is often associated with H_2 generated in this reaction. Thus, in the case of lower space velocity, more H_2 is generated than at higher space velocity. This additional hydrogen might be the answer to the disparity between amount of coke and corresponding activity for Mo/SZ catalysts similar to Mo/H-ZSM-5 [53, 64-66].

Comparison with Literature

A comparison of Mo/SZ with Mo supported on different supports from the literature is shown in **Table 3**. This shows that benzene yield on Mo/SZ at 650^{o}C is comparable to Mo/H-ZSM-5 at 675 ^{o}C. At 700 ^{o}C, benzene and the overall aromatics yield for Mo/H-ZSM-5 are far greater compared to Mo/SZ. Compared to other acidic supports such as H-Mordenite or H-SSZ-13 that possess strong acidity, sulfated zirconia shows greater benzene yields (Table 3). Although, this is not a direct comparison because physical/chemical factors such as pretreatment, space velocity, Mo content can contribute to this difference. For example, the sulfate may not be stable at temperatures 700 ^{o}C, and the lack of shape selectivity [34] in sulfated zirconia, may affect the comparison of Mo/SZ and the literature.

Although Mo/SZ has no shape selectivity, the strong acidity in SZ is sufficient to catalyze the aromatization reaction. The literature shows that benzene selectivities on Mo/H-ZSM-5 are 50-90% and thus, is more active for aromatization of methane to benzene than Mo/SZ. Mo/SZ is more selective for non-oxidative conversion of methane to heavier aromatics such as naphthalene and coke.

Temperature Programmed Oxidation (TPO)

Figure shows TPO results for 1 % and 5 % Mo/SZ catalysts. There are distinct differences among the two spent catalysts, as expected due to different activities of methane DHA. Based on the TPO peak temperatures, the coke on both catalysts can be described as either amorphous or soft coke, corresponding to peak temperatures of ~ 400 ^{o}C [67] or polymeric, and hard coke corresponding to peak temperatures of ~ 500-600 ^{o}C [68]. This hard coke is often associated with deactivation of strong BAS. The TPO results for the 1% and 5% Mo/SZ catalysts showed similar pattern of peak TPO positions. For 1% Mo/SZ, there is one large peak at ~ 590 ^{o}C while one at ~510 ^{o}C for 5% Mo/SZ. Both can be attributed to polymeric coke. This shift in peak positions is attributable to the amount of acidity of the catalyst (NH_3-TPD results). More acidity might correspond to higher peak oxidation temperature [68]. For 1% Mo/SZ, an

identifiable small peak can be seen at ~ 440 ^{o}C, which can be designated as amorphous coke [67]. Another small peak at ~ 685 ^{o}C for the 5% Mo/SZ can be designated as graphitic coke. Overall, 5% Mo/SZ catalyst that showed greater activity in DHA but also greater amounts of coke (**Table 4**).

Conclusions

Supported Mo/SZ catalyst is active for the DHA reaction. SEM-EDS and ICP-OES confirmed the actual loading of 1%, and 5% Mo on SZ. Pyridine-based DRIFTS and NH_3-TPD analysis shows that both Brønsted and Lewis sites are present on these catalysts. Further analysis confirmed that Mo loading did not significantly affect acidity. At the higher 5% Mo loading, more Lewis acid sites were observed than SZ, however BAS were weakened by the addition of Mo, possibly due to interaction between sulfate and Mo. Higher loadings of Mo resulted in lower total acidity. The presence of the apparent active sites, MoO_xC_y were confirmed through XANES, XPS, and HRTEM. Mo loading strongly influenced the dispersion and number of available sites for methane activation. It appears that the loss of sulfate content and significant coking leads to deactivation of the catalysts. A literature comparison of benzene selectivities shows that Mo/H-ZSM-5 is far more active than Mo/SZ. Mo/SZ was found to be more selective for non-oxidative conversion of methane to heavier aromatics such as naphthalene and coke.

Acknowledgements

Authors would like to acknowledge financial support for this work from LSU's Office of Research and Economic Development (ORED). Authors would like to thank Dr. Amitava Roy from LSU's CAMD synchrotron source for help with Mo 'K' and 'L' edge experiments. Authors would also like to thank Dr. Clayton Loehn, and Dr. Dongmei Cao from LSU SIF for help with the characterization experiments (XPS, SEM, TEM, Raman). Authors would also like to thank Dr.

Tommy Blanchard from LSU Oceanography and Ms. Wanda Leblanc from LSU Geology for help with ICP-OES analysis.

References

[1] R.S. Middleton, R. Gupta, J.D. Hyman, H.S. Viswanathan, The shale gas revolution: Barriers, sustainability, and emerging opportunities, Applied Energy, 199 (2017) 88-95.
[2] A. Press, CO2 emissions in U.S. drop to 20-year low, in, Politico, 2012.
[3] G.E. Keller, M.M. Bhasin, Synthesis of ethylene via oxidative coupling of methane, Journal of Catalysis, 73 (1982) 9-19.
[4] N. Kumar, Z. Wang, S. Kanitkar, J.J. Spivey, Methane reforming over Ni-based pyrochlore catalyst: deactivation studies for different reactions, Applied Petrochemical Research, (2016) 1-7.
[5] D. Pakhare, J. Spivey, A review of dry (CO2) reforming of methane over noble metal catalysts, Chemical Society Reviews, 43 (2014) 7813-7837.
[6] G.A. Olah, A. Goeppert, M. Czaun, G.K.S. Prakash, Bi-reforming of Methane from Any Source with Steam and Carbon Dioxide Exclusively to Metgas (CO–2H2) for Methanol and Hydrocarbon Synthesis, Journal of the American Chemical Society, 135 (2013) 648-650.
[7] V.R. Choudhary, K.C. Mondal, T.V. Choudhary, Oxy-methane reforming over high temperature stable NiCoMgCeOx and NiCoMgOx supported on zirconia–haffnia catalysts: Accelerated sulfur deactivation and regeneration, Catalysis Communications, 8 (2007) 561-564.
[8] B. Christian Enger, R. Lødeng, A. Holmen, A review of catalytic partial oxidation of methane to synthesis gas with emphasis on reaction mechanisms over transition metal catalysts, Applied Catalysis A: General, 346 (2008) 1-27.
[9] A. Zhang, S. Sun, Z.J.A. Komon, N. Osterwalder, S. Gadewar, P. Stoimenov, D.J. Auerbach, G.D. Stucky, E.W. McFarland, Improved light olefin yield from methyl bromide coupling over modified SAPO-34 molecular sieves, Physical Chemistry Chemical Physics, 13 (2011) 2550-2555.
[10] Q. Zhu, S.L. Wegener, C. Xie, O. Uche, M. Neurock, T.J. Marks, Sulfur as a selective 'soft' oxidant for catalytic methane conversion probed by experiment and theory, Nat Chem, 5 (2013) 104-109.
[11] A. Iulianelli, S. Liguori, J. Wilcox, A. Basile, Advances on methane steam reforming to produce hydrogen through membrane reactors technology: A review, Catalysis Reviews, 58 (2016) 1-35.
[12] G.A. Olah, G. Klopman, R.H. Schlosberg, Super acids. III. Protonation of alkanes and intermediacy of alkanonium ions, pentacoordinated carbon cations of CH5+ type. Hydrogen exchange, protolytic cleavage, hydrogen abstraction; polycondensation of methane, ethane, 2,2-dimethylpropane and 2,2,3,3-tetramethylbutane in FSO3H-SbF5, Journal of the American Chemical Society, 91 (1969) 3261-3268.
[13] G.A. Olah, R.H. Schlosberg, Chemistry in super acids. I. Hydrogen exchange and polycondensation of methane and alkanes in FSO3H-SbF5 ("magic acid") solution. Protonation of alkanes and the intermediacy of CH5+ and related hydrocarbon ions. The high chemical reactivity of "paraffins" in ionic solution reactions, Journal of the American Chemical Society, 90 (1968) 2726-2727.
[14] S. Vasireddy, S. Ganguly, J. Sauer, W. Cook, J.J. Spivey, Direct conversion of methane to higher hydrocarbons using AlBr3-HBr superacid catalyst, Chemical Communications, 47 (2011) 785-787.
[15] W. Hua, A. Goeppert, J. Sommer, Methane activation in the presence of Al2O3-promoted sulfated zirconia, Applied Catalysis A: General, 219 (2001) 201-207.
[16] D. Fraenkel, Methane conversion over sulfated zirconia, Catalysis Letters, 58 (1999) 123-125.
[17] S. Rezgui, A. Liang, T.K. Cheung, B.C. Gates, Methane conversion to ethane in the presence of iron- and manganese-promoted sulfated zirconia, Catalysis Letters, 53 (1998) 1-2.

[18] X. Guo, G. Fang, G. Li, H. Ma, H. Fan, L. Yu, C. Ma, X. Wu, D. Deng, M. Wei, D. Tan, R. Si, S. Zhang, J. Li, L. Sun, Z. Tang, X. Pan, X. Bao, Direct, Nonoxidative Conversion of Methane to Ethylene, Aromatics, and Hydrogen, Science, 344 (2014) 616-619.
[19] D. Wang, J.H. Lunsford, M.P. Rosynek, Catalytic conversion of methane to benzene over Mo/ZSM-5, Topics in Catalysis, 3 (1996) 289-297.
[20] L. Wang, L. Tao, M. Xie, G. Xu, J. Huang, Y. Xu, Dehydrogenation and aromatization of methane under non-oxidizing conditions, Catalysis Letters, 21 (1993) 35-41.
[21] L. Wang, R. Ohnishi, M. Ichikawa, Selective Dehydroaromatization of Methane toward Benzene on Re/HZSM-5 Catalysts and Effects of CO/CO2 Addition, Journal of Catalysis, 190 (2000) 276-283.
[22] A.A. Gabrienko, S.S. Arzumanov, A.V. Toktarev, I.G. Danilova, I.P. Prosvirin, V.V. Kriventsov, V.I. Zaikovskii, D. Freude, A.G. Stepanov, Different Efficiency of Zn2+ and ZnO Species for Methane Activation on Zn-Modified Zeolite, ACS Catalysis, 7 (2017) 1818-1830.
[23] A.A. Gabrienko, S.S. Arzumanov, M.V. Luzgin, A.G. Stepanov, V.N. Parmon, Methane Activation on Zn2+-Exchanged ZSM-5 Zeolites. The Effect of Molecular Oxygen Addition, The Journal of Physical Chemistry C, 119 (2015) 24910-24918.
[24] L. Li, S. Fan, X. Mu, Z. Mi, C.-J. Li, Photoinduced Conversion of Methane into Benzene over GaN Nanowires, Journal of the American Chemical Society, 136 (2014) 7793-7796.
[25] J. Oró, J. Han, High-Temperature Synthesis of Aromatic Hydrocarbons from Methane, Science, 153 (1966) 1393.
[26] J.J. Spivey, G. Hutchings, Catalytic aromatization of methane, Chemical Society Reviews, 43 (2014) 792-803.
[27] Z.R. Ismagilov, E.V. Matus, L.T. Tsikoza, Direct conversion of methane on Mo/ZSM-5 catalysts to produce benzene and hydrogen: achievements and perspectives, Energy & Environmental Science, 1 (2008) 526-541.
[28] K. Sun, D.M. Ginosar, T. He, Y. Zhang, M. Fan, R. Chen, Progress in Nonoxidative Dehydroaromatization of Methane in the Last 6 Years, Industrial & Engineering Chemistry Research, 57 (2018) 1768-1789.
[29] I. Vollmer, I. Yarulina, F. Kapteijn, J. Gascon, Progress in Developing a Structure-Activity Relationship for the Direct Aromatization of Methane, ChemCatChem, 0 (2018).
[30] A. Kumar, K. Song, L. Liu, Y. Han, A. Bhan, Absorptive Hydrogen Scavenging for Enhanced Aromatics Yield During Non-oxidative Methane Dehydroaromatization on Mo/H-ZSM-5 Catalysts, Angewandte Chemie International Edition, 57 (2018) 15577-15582.
[31] N. Kosinov, F.J.A.G. Coumans, G. Li, E. Uslamin, B. Mezari, A.S.G. Wijpkema, E.A. Pidko, E.J.M. Hensen, Stable Mo/HZSM-5 methane dehydroaromatization catalysts optimized for high-temperature calcination-regeneration, Journal of Catalysis, 346 (2017) 125-133.
[32] M. Agote-Arán, A.B. Kroner, H.U. Islam, W.A. Sławiński, D.S. Wragg, I. Lezcano-González, A.M. Beale, Determination of Molybdenum Species Evolution during Non-Oxidative Dehydroaromatization of Methane and its Implications for Catalytic Performance, ChemCatChem, 0.
[33] L.G. Inés, O. Ramon, R. Mauro, G. Pieter, B.S. W., W.B. M., B.A. M., Molybdenum Speciation and its Impact on Catalytic Activity during Methane Dehydroaromatization in Zeolite ZSM-5 as Revealed by Operando X-Ray Methods, Angewandte Chemie, 128 (2016) 5301-5305.
[34] N. Kosinov, F.J.A.G. Coumans, E.A. Uslamin, A.S.G. Wijpkema, B. Mezari, E.J.M. Hensen, Methane Dehydroaromatization by Mo/HZSM-5: Mono- or Bifunctional Catalysis?, ACS Catalysis, 7 (2017) 520-529.
[35] Y. Luo, Z. Mei, N. Liu, H. Wang, C. Han, S. He, Synthesis of mesoporous sulfated zirconia nanoparticles with high surface area and their applies for biodiesel production as effective catalysts, Catalysis Today, 298 (2017) 99-108.
[36] K.M. Arata, H., Solid Superacids, Nova Science Publishers, New York, 2011.

[37] B.M. Reddy, M.K. Patil, Organic Syntheses and Transformations Catalyzed by Sulfated Zirconia, Chemical Reviews, 109 (2009) 2185-2208.
[38] F.F. Oloye, A.J. McCue, J.A. Anderson, n-Heptane hydroconversion over sulfated-zirconia-supported molybdenum carbide catalysts, Applied Petrochemical Research, 6 (2016) 341-352.
[39] N. Katada, J.-i. Endo, K.-i. Notsu, N. Yasunobu, N. Naito, M. Niwa, Superacidity and Catalytic Activity of Sulfated Zirconia, The Journal of Physical Chemistry B, 104 (2000) 10321-10328.
[40] E.A. El-Sharkawy, A.S. Khder, A.I. Ahmed, Structural characterization and catalytic activity of molybdenum oxide supported zirconia catalysts, Microporous and Mesoporous Materials, 102 (2007) 128-137.
[41] A.S.C. Brown, J.S.J. Hargreaves, S.H. Taylor, A study of "superacidic" MoO3/ZrO2 catalysts for methane oxidation, Catalysis Letters, 57 (1999) 109-113.
[42] T.-c. Xiao, A.P.E. York, V.C. Williams, H. Al-Megren, A. Hanif, X.-y. Zhou, M.L.H. Green, Preparation of Molybdenum Carbides Using Butane and Their Catalytic Performance, Chemistry of Materials, 12 (2000) 3896-3905.
[43] A.C. Ferrari, Raman spectroscopy of graphene and graphite: Disorder, electron–phonon coupling, doping and nonadiabatic effects, Solid State Communications, 143 (2007) 47-57.
[44] J. Schwan, S. Ulrich, V. Batori, H. Ehrhardt, S.R.P. Silva, Raman spectroscopy on amorphous carbon films, Journal of Applied Physics, 80 (1996) 440-447.
[45] E.P. Parry, An infrared study of pyridine adsorbed on acidic solids. Characterization of surface acidity, Journal of Catalysis, 2 (1963) 371-379.
[46] W.-H. Chen, H.-H. Ko, A. Sakthivel, S.-J. Huang, S.-H. Liu, A.-Y. Lo, T.-C. Tsai, S.-B. Liu, A solid-state NMR, FT-IR and TPD study on acid properties of sulfated and metal-promoted zirconia: Influence of promoter and sulfation treatment, Catalysis Today, 116 (2006) 111-120.
[47] B. Li, S. Li, N. Li, H. Chen, W. Zhang, X. Bao, B. Lin, Structure and acidity of Mo/ZSM-5 synthesized by solid state reaction for methane dehydrogenation and aromatization, Microporous and Mesoporous Materials, 88 (2006) 244-253.
[48] W. Liu, Y. Xu, Methane Dehydrogenation and Aromatization over Mo/HZSM-5: In Situ FT–IR Characterization of Its Acidity and the Interaction between Mo Species and HZSM-5, Journal of Catalysis, 185 (1999) 386-392.
[49] T.A. Patterson, J.C. Carver, D.E. Leyden, D.M. Hercules, A surface study of cobalt-molybdena-alumina catalysts using x-ray photoelectron spectroscopy, The Journal of Physical Chemistry, 80 (1976) 1700-1708.
[50] T.H. Fleisch, G.J. Mains, An XPS study of the UV reduction and photochromism of MoO3 and WO3, The Journal of chemical physics, 76 (1982) 780-786.
[51] K. Suzuki, M. Soma, T. Onishi, K. Tamaru, Reactivity of molybdenum disulfide surfaces studied by XPS, Journal of Electron Spectroscopy and Related Phenomena, 24 (1981) 283-287.
[52] W. Ding, S. Li, G. D Meitzner, E. Iglesia, Methane Conversion to Aromatics on Mo/H-ZSM5: Structure of Molybdenum Species in Working Catalysts, The Journal of Physical Chemistry B, 105 (2001) 506-513.
[53] H. Aritani, H. Shibasaki, H. Orihara, A. Nakahira, Methane dehydroaromatization over Mo-modified H-MFI for gas to liquid catalysts, Journal of Environmental Sciences, 21 (2009) 736-740.
[54] E.V. Matus, I.Z. Ismagilov, O.B. Sukhova, V.I. Zaikovskii, L.T. Tsikoza, Z.R. Ismagilov, J.A. Moulijn, Study of Methane Dehydroaromatization on Impregnated Mo/ZSM-5 Catalysts and Characterization of Nanostructured Molybdenum Phases and Carbonaceous Deposits, Industrial & Engineering Chemistry Research, 46 (2007) 4063-4074.
[55] Z.R.M. Ismagilov, E. V.; Ismagilova, I. Z.; Kerzhentseva, I. Z.; Zailovskiia, V. I.; Dosumovb, K. D.; Mustafinc, A. G. , Structural Changes of Mo/ZSM-5 Catalysts During the Methane Dehydroaromatization, Eurasian Chemico Technological Journal, 12 (2010) 9-16.

[56] S.R.J. Likith, C.A. Farberow, S. Manna, A. Abdulslam, V. Stevanović, D.A. Ruddy, J.A. Schaidle, D.J. Robichaud, C.V. Ciobanu, Thermodynamic Stability of Molybdenum Oxycarbides Formed from Orthorhombic Mo2C in Oxygen-Rich Environments, The Journal of Physical Chemistry C, 122 (2018) 1223-1233.
[57] P. Delporte, F.d.r. Meunier, C. Pham-Huu, P. Vennegues, M.J. Ledoux, J. Guille, Physical characterization of molybdenum oxycarbide catalyst; TEM, XRD and XPS, Catalysis Today, 23 (1995) 251-267.
[58] E.V. Matus, O.B. Sukhova, I.Z. Ismagilov, L.T. Tsikoza, Z.R. Ismagilov, Peculiarities of dehydroaromatization of CH4-C2H6 and CH4 over Mo/ZSM-5 catalysts, React. Kinet. Catal. Lett., 98 (2009) 59-67.
[59] C.H.L. Tempelman, E.J.M. Hensen, On the deactivation of Mo/HZSM-5 in the methane dehydroaromatization reaction, Applied Catalysis B: Environmental, 176-177 (2015) 731-739.
[60] S.J. Han, S.K. Kim, A. Hwang, S. Kim, D.-Y. Hong, G. Kwak, K.-W. Jun, Y.T. Kim, Non-oxidative dehydroaromatization of methane over Mo/H-ZSM-5 catalysts: A detailed analysis of the reaction-regeneration cycle, Applied Catalysis B: Environmental, 241 (2019) 305-318.
[61] R. Srinivasan, R.A. Keogh, D.R. Milburn, B.H. Davis, Sulfated Zirconia Catalysts: Characterization by TGA/DTA Mass Spectrometry, Journal of Catalysis, 153 (1995) 123-130.
[62] M. Bi, H. Li, W.-P. Pan, W.G. Lloyd, Thermal studies of metal promoted sulfated zirconia, (1996).
[63] C. Karakaya, S.H. Morejudo, H. Zhu, R.J. Kee, Catalytic Chemistry for Methane Dehydroaromatization (MDA) on a Bifunctional Mo/HZSM-5 Catalyst in a Packed Bed, Industrial & Engineering Chemistry Research, 55 (2016) 9895-9906.
[64] Y. Xu, Y. Song, Y. Suzuki, Z.-G. Zhang, Effect of superficial velocity on the coking behavior of a nanozeolite-based Mo/HZSM-5 catalyst in the non-oxidative CH4 dehydroaromatization at 1073 K, Catalysis Science & Technology, 3 (2013) 2769-2777.
[65] K. Skutil, M. Taniewski, Some technological aspects of methane aromatization (direct and via oxidative coupling), Fuel Processing Technology, 87 (2006) 511-521.
[66] H. Ma, R. Ohnishi, M. Ichikawa, Highly Stable Performance of Methane Dehydroaromatization on Mo/HZSM-5 Catalyst with a Small Amount of H2 Addition into Methane Feed, Catalysis Letters, 89 (2003) 143-146.
[67] C.A. Querini, Coke characterization, in: J.J. Spivey, G.W. Roberts (Eds.) Catalysis: Volume 17, The Royal Society of Chemistry, 2004, pp. 166-209.
[68] F. Denardin, O.W. Perez-Lopez, Tuning the acidity and reducibility of Fe/ZSM-5 catalysts for methane dehydroaromatization, Fuel, 236 (2019) 1293-1300.

Figure 1: Oxidative conversion routes of methane to higher hydrocarbons

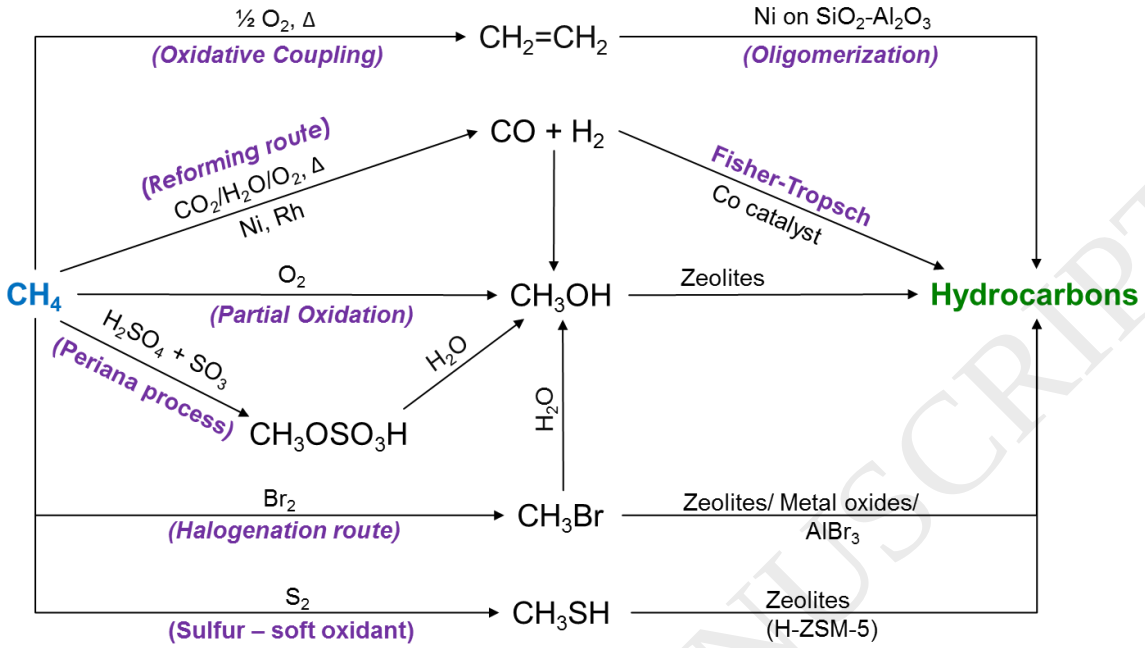

Figure 2: Raman spectra for samples at various treatment (a) base SZ, (b) fresh 5%Mo/SZ, (c) carburized 5%Mo/SZ, (d) spent 5%Mo/SZ

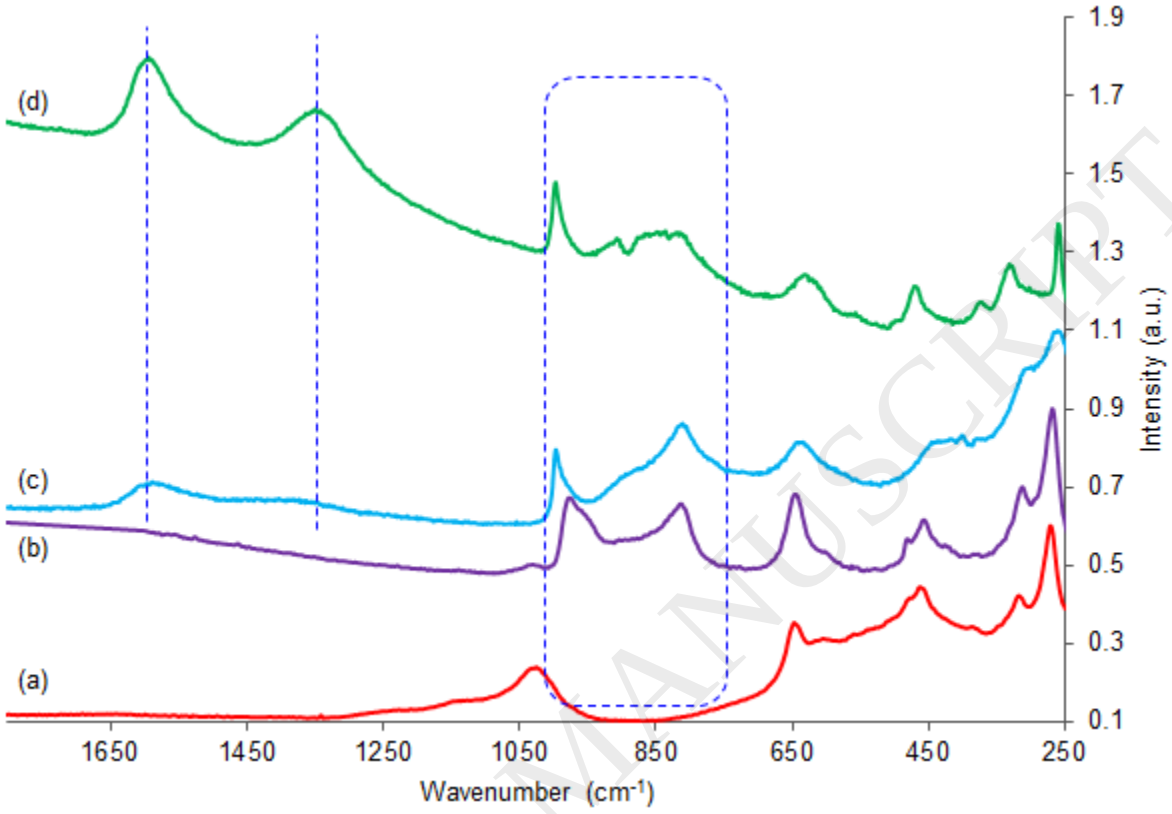

Figure 3: Comparison of SZ and Mo doped SZ catalysts after pyridine desorption at 100 ^{0}C (a) SZ, (b) 1% Mo/SZ, (c) 5% Mo/SZ, “B” = Bronsted, “L” = Lewis

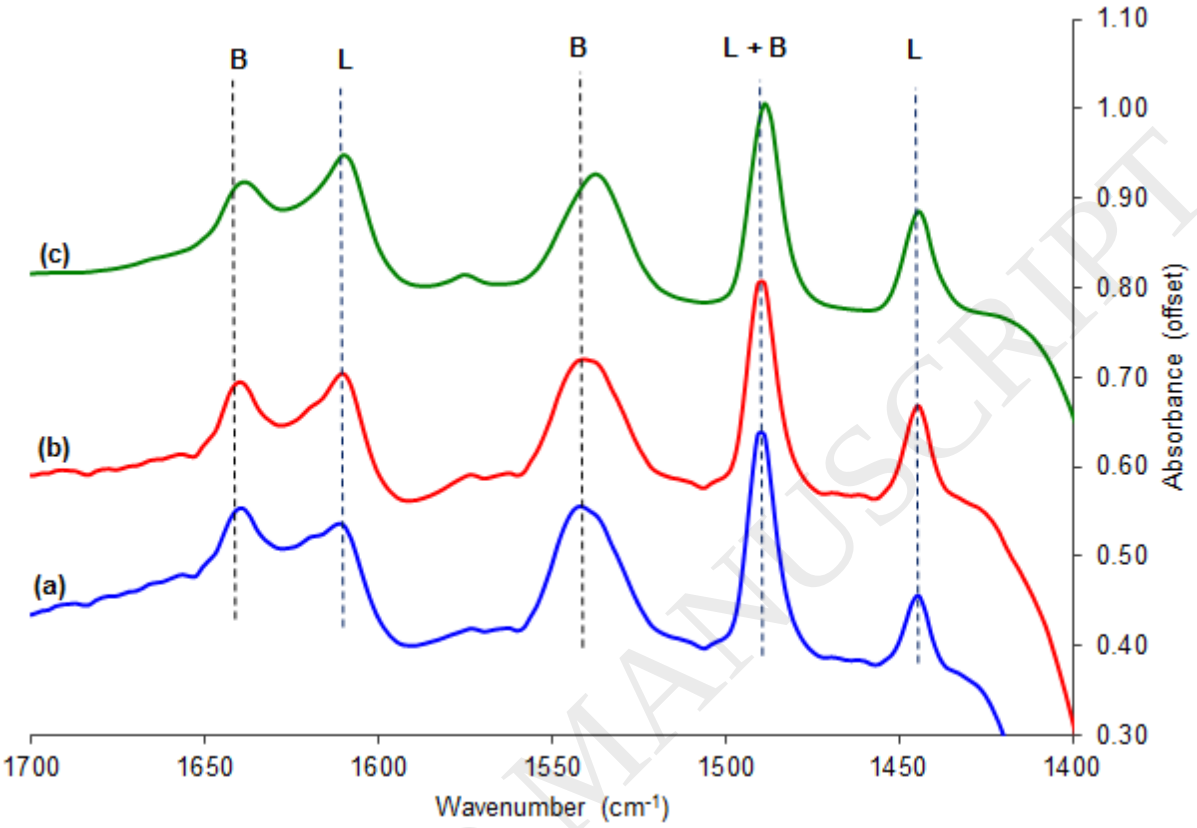

Figure 4: NH_3-TPD comparison for all the catalysts (a) SZ, (b) 1% Mo/SZ, and (c) 5% Mo/SZ. Values next to each curve represent quantity of NH_3 desorbed per gram of catalyst

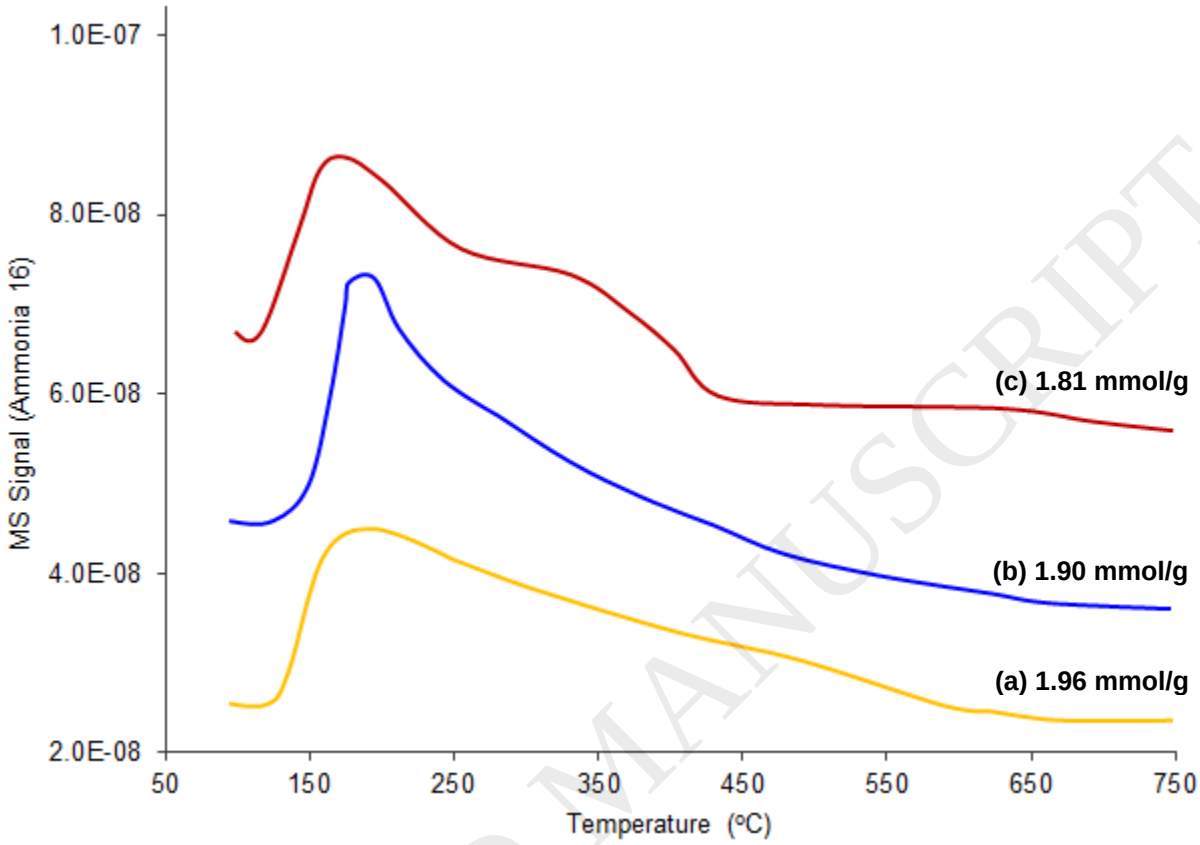

Figure 5: XPS comparison of Mo 3d for (a) MoO_3 std., (b) Fresh 5%Mo/SZ (oxide form), (c) Carburized 5% Mo/SZ, (d) Spent 5%Mo/SZ (after reaction for 1000 min at 650 ^{0}C), (e) β-Mo_2C std., (f) MoO_2 std., (g) MoS_2 std., (h) Mo metal powder std.

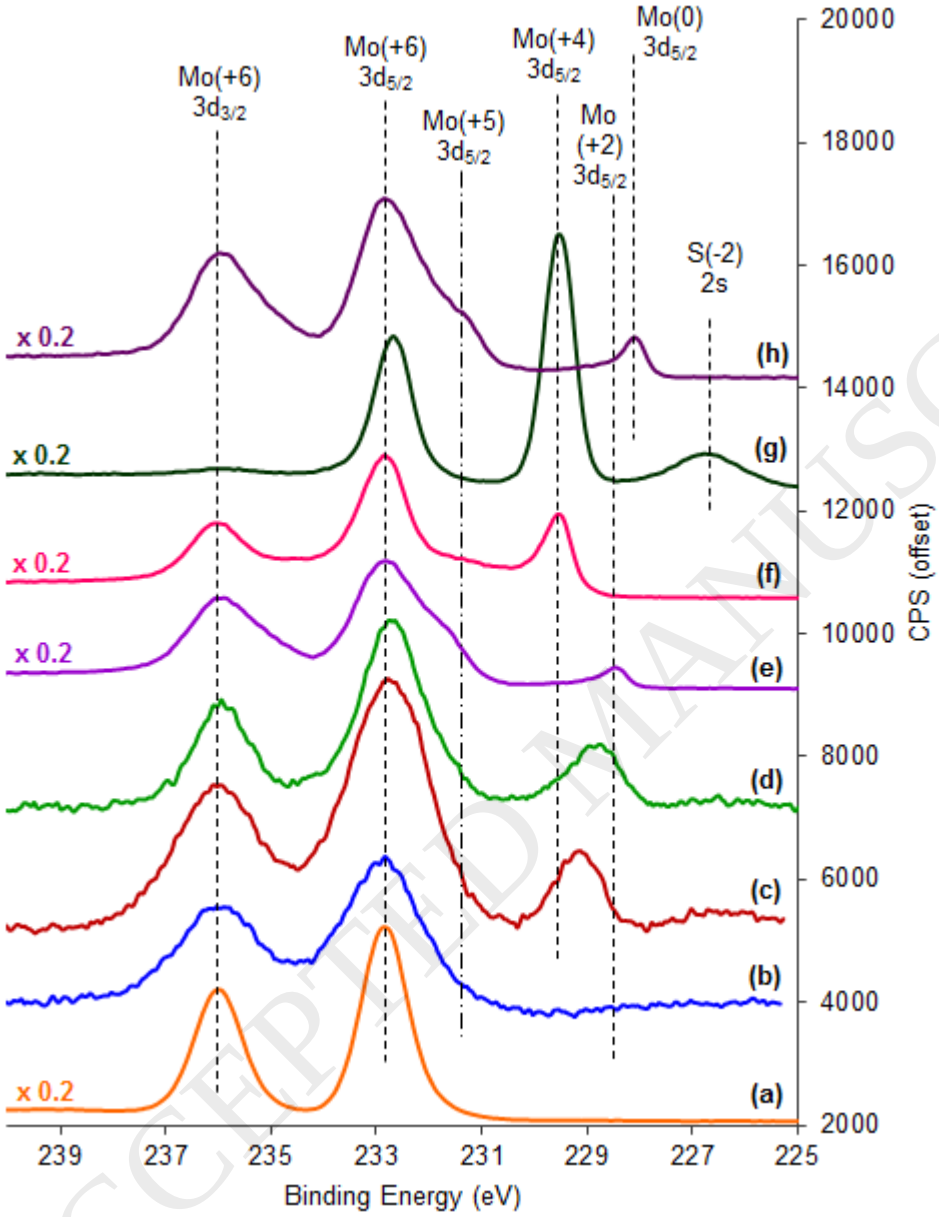

Figure 6: K-edge XANES spectra for catalyst samples: (a) MoO_3 – std., (b) Fresh 5%Mo/SZ (oxidized form), (c) Carburized 5%Mo/SZ, (d) Spent 5%Mo/SZ, (e) Mo_2C-std.

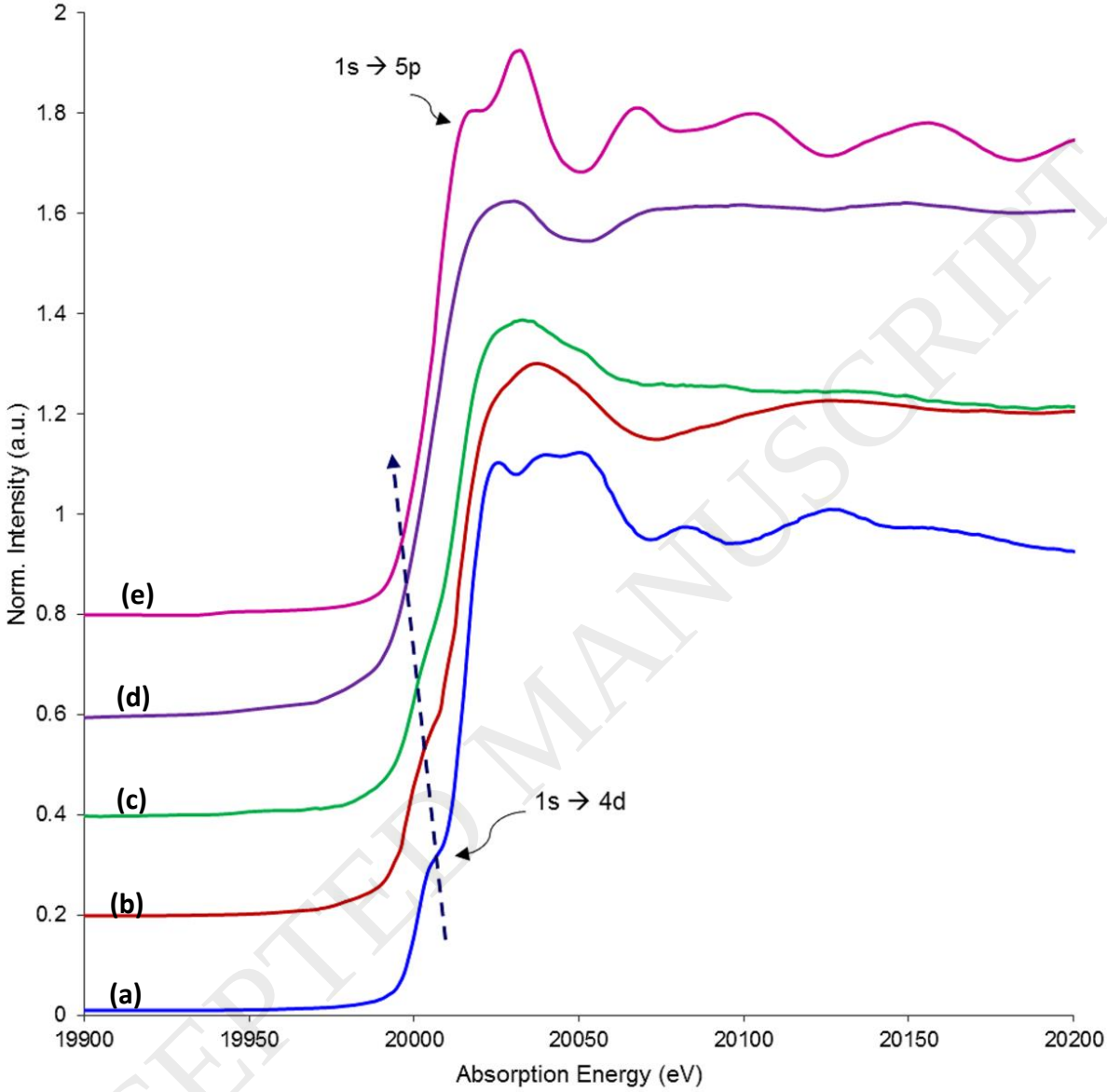

Figure 7: HRTEM for base sulfated zirconia (SZ)

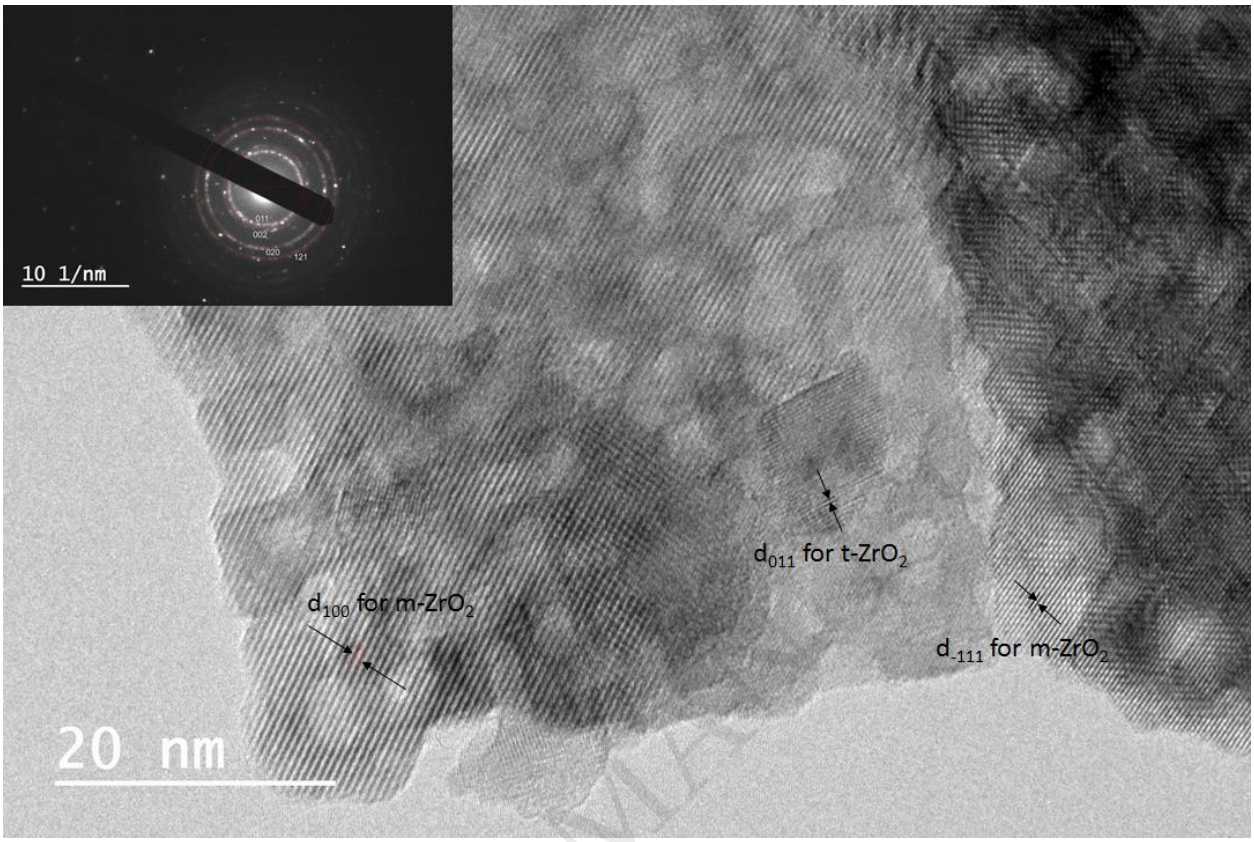

Figure 8: HRTEM for fresh 5% Mo/SZ catalyst

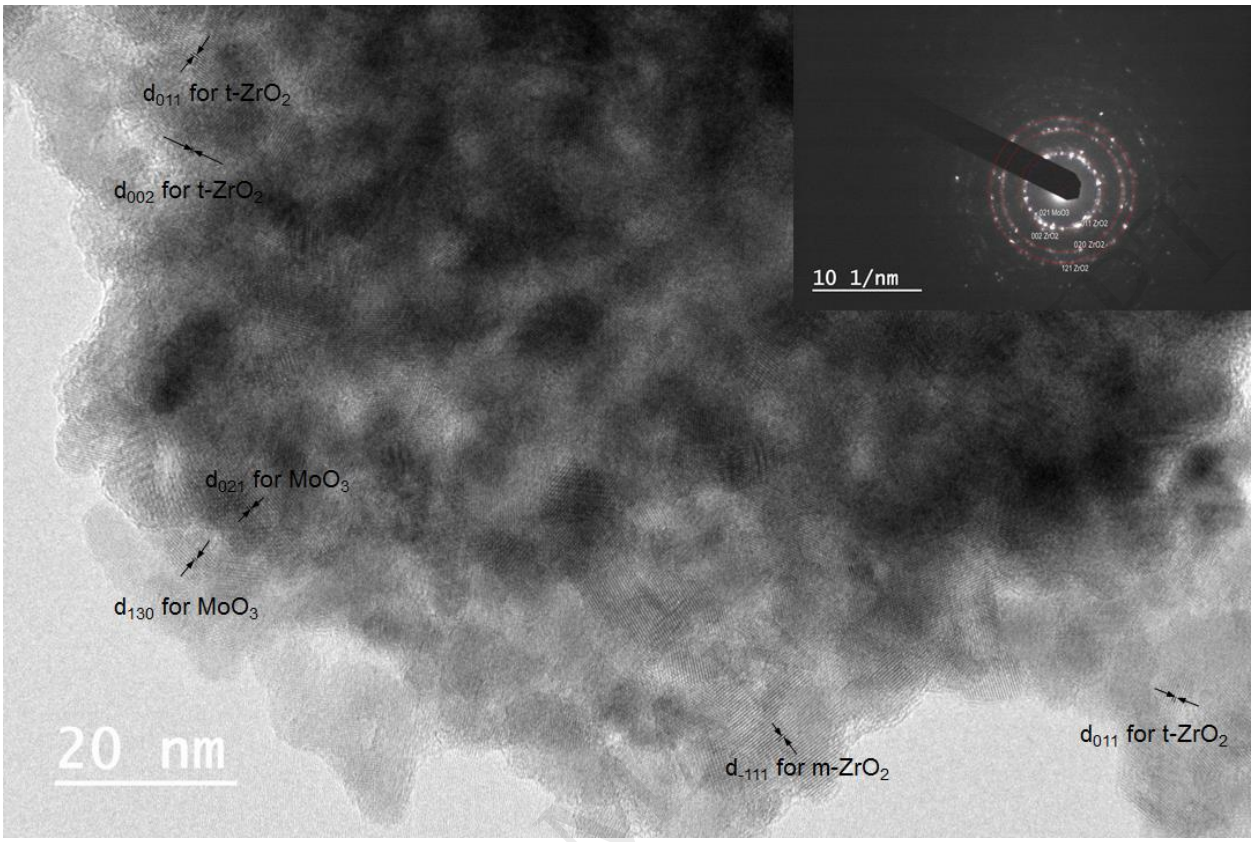

Figure 9: HRTEM for carburized 5% Mo/SZ catalyst

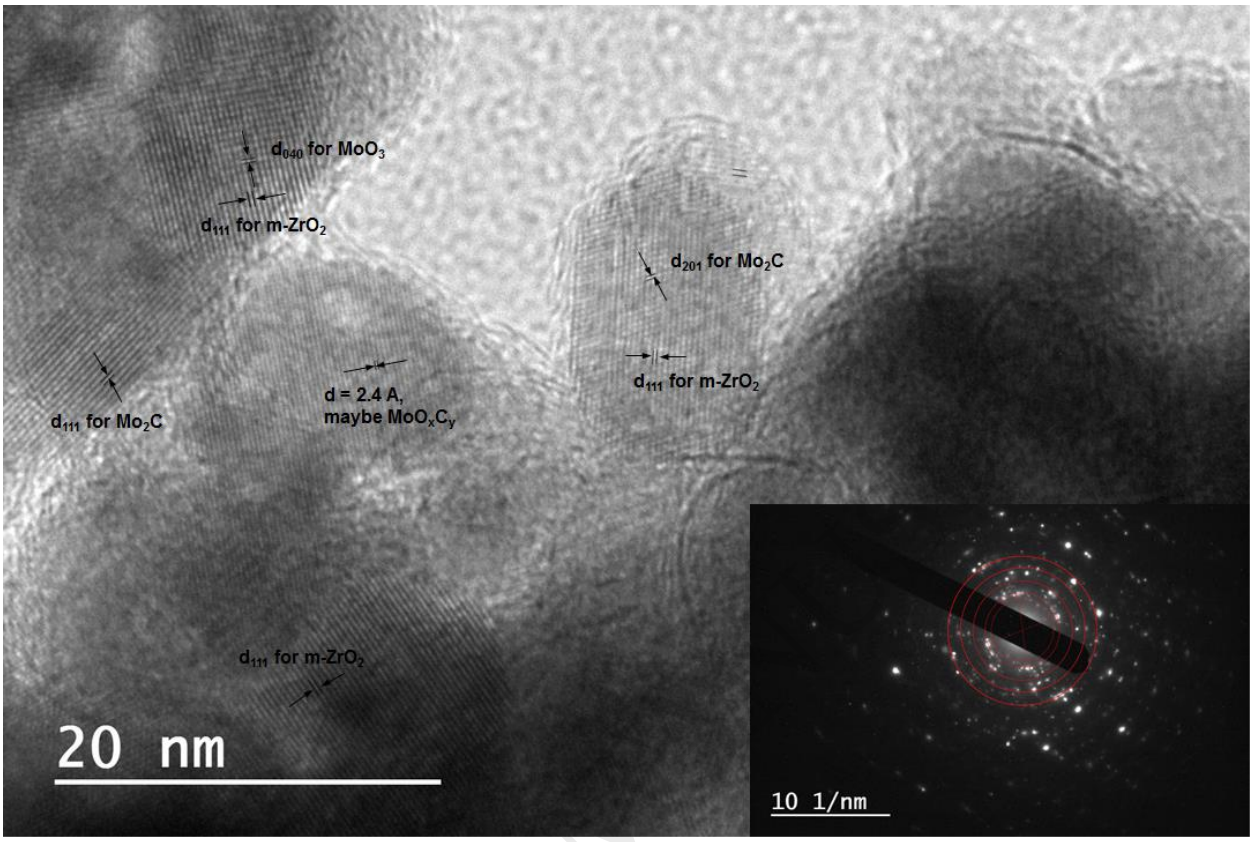

Figure 10: HRTEM for spent 5% Mo/SZ catalyst

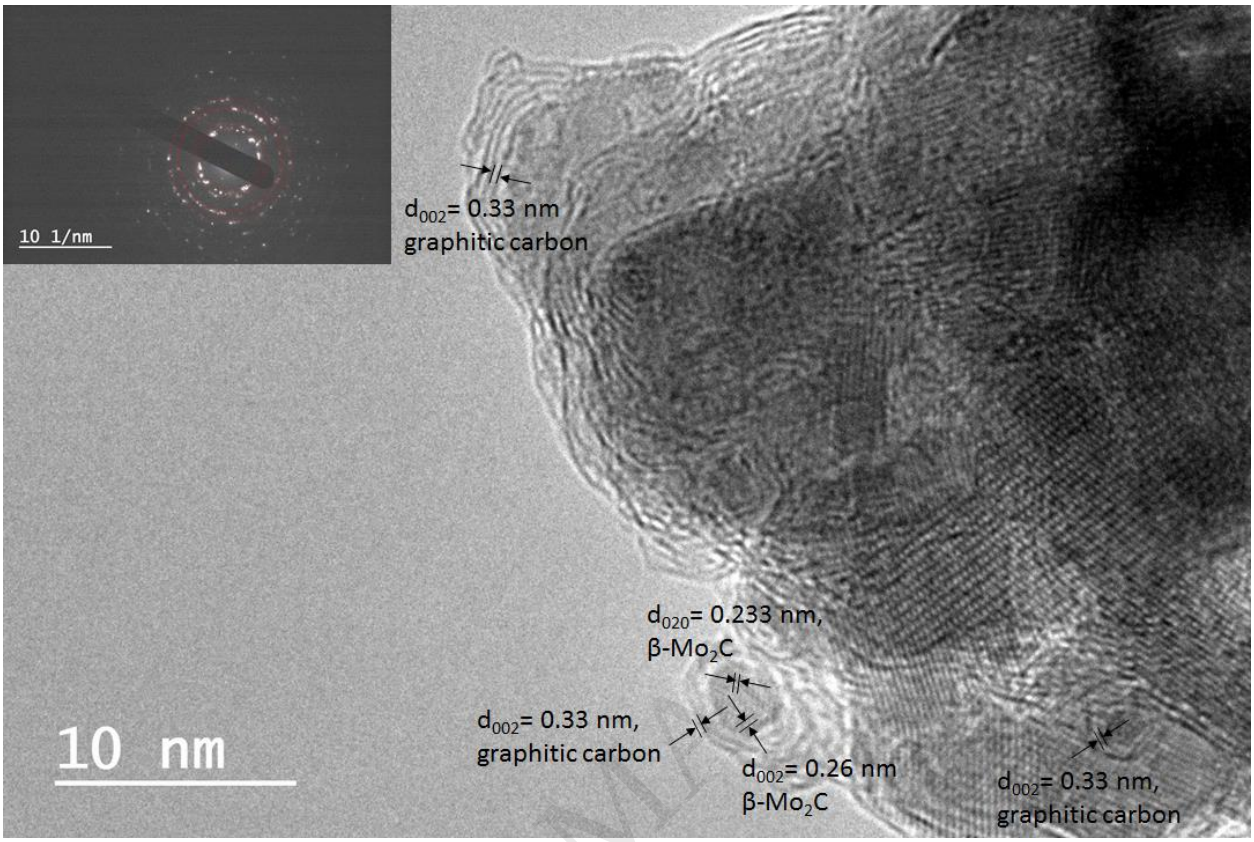

Figure 11: Reaction data for methane DHA over 1% Mo/SZ catalyst (650 ^{o}C, 1 atm, 0.6 L.gcat^{-1}.hr^{-1}). *Npt = Naphthalene

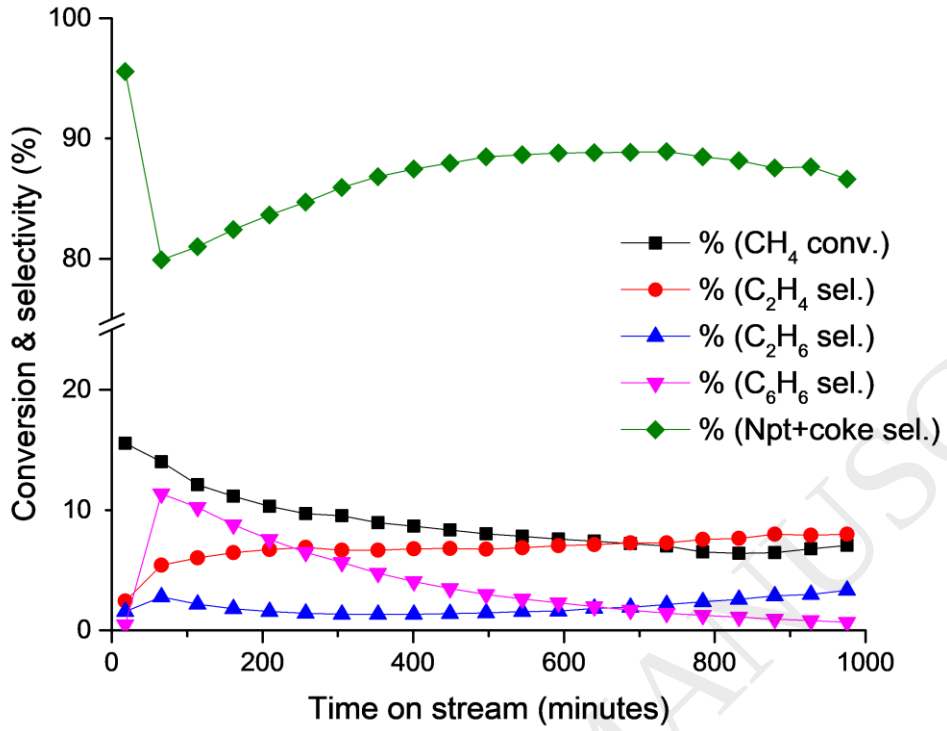

Figure 12 Reaction data for methane DHA over 5% Mo/SZ catalyst (650 ^{o}C, 1 atm, 600 ml/gcat-hr)

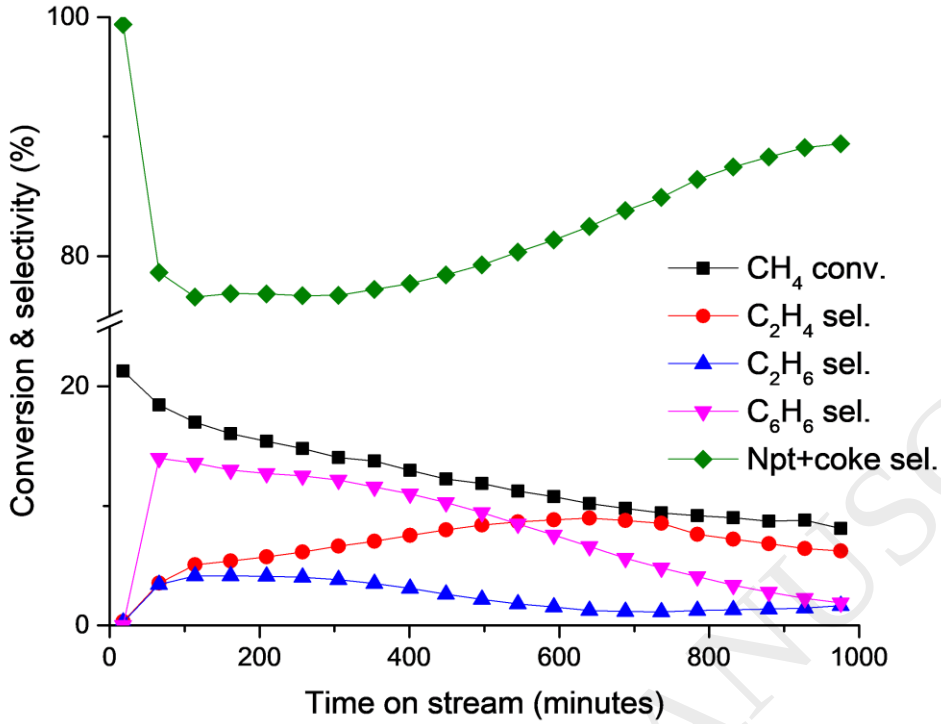

Figure 13: Effect of temperature on ethylene selectivity over 5% Mo/SZ catalyst (0.6 L.gcat^{-1}.hr^{-1}, 1 atm)

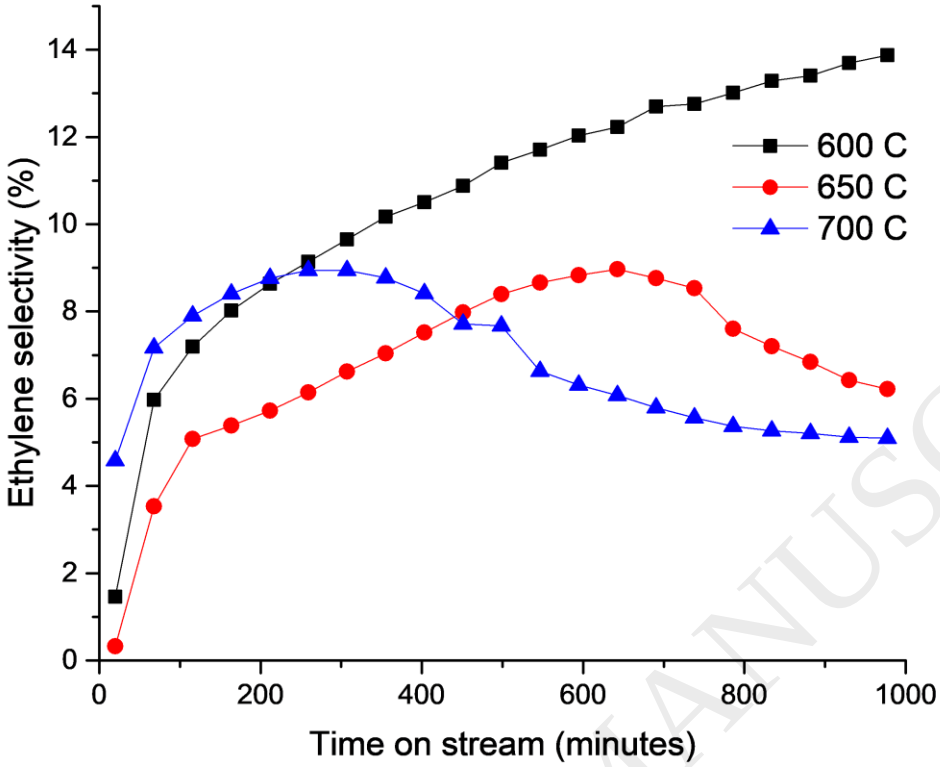

Figure 14: Effect of temperature on benzene selectivity over 5% Mo/SZ catalyst (1 atm, 0.6 $L.gcat^{-1}.hr^{-1}$)

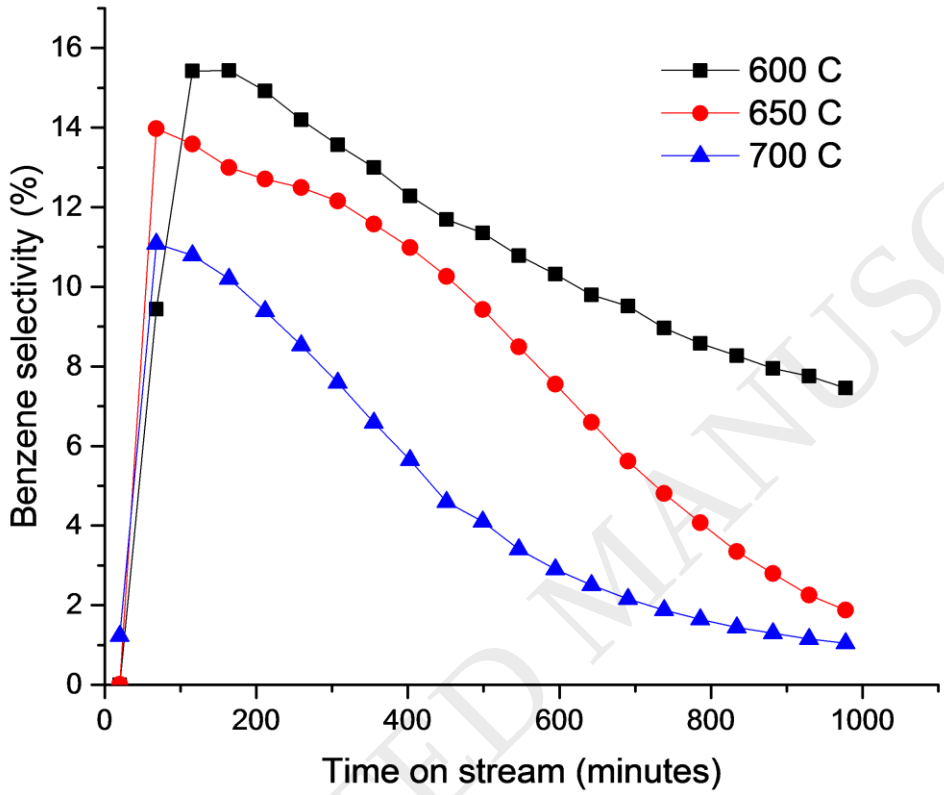

Figure 15: Effect of space velocity on CH_4 conversion over 5% Mo/SZ catalyst (650 ^oC, 1 atm). Space velocity (SV) has units of $L.gcat^{-1}.hr^{-1}$.

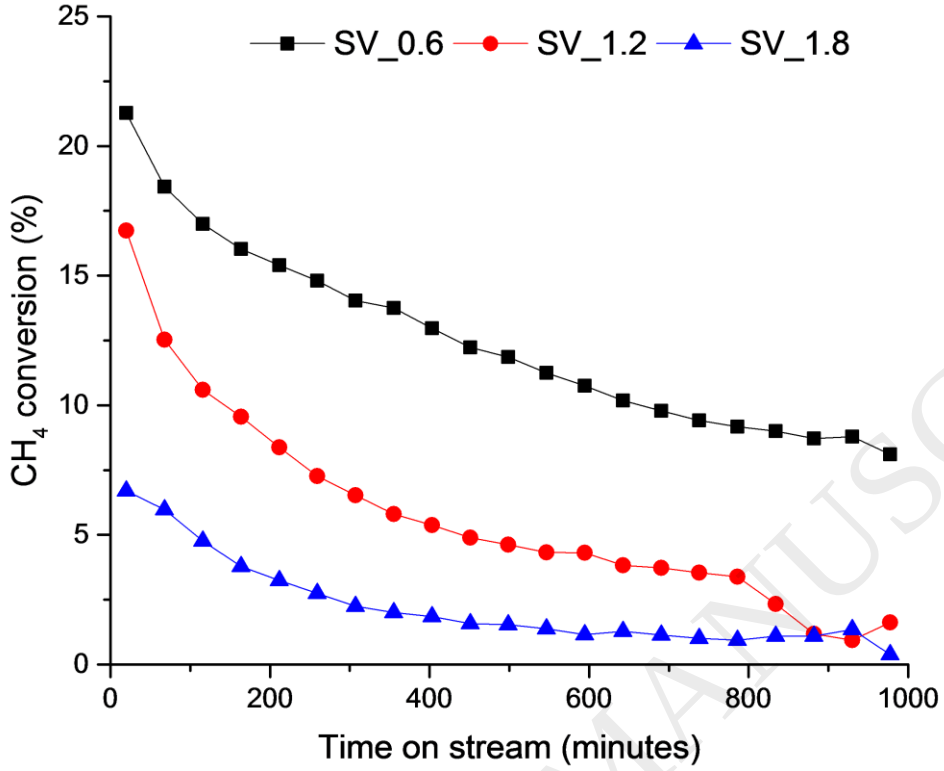

Figure 16: Effect of space velocity on ethylene selectivity over 5% Mo/SZ catalyst (650 ^{o}C, 1 atm). SV has units of L.gcat^{-1}.hr^{-1}.

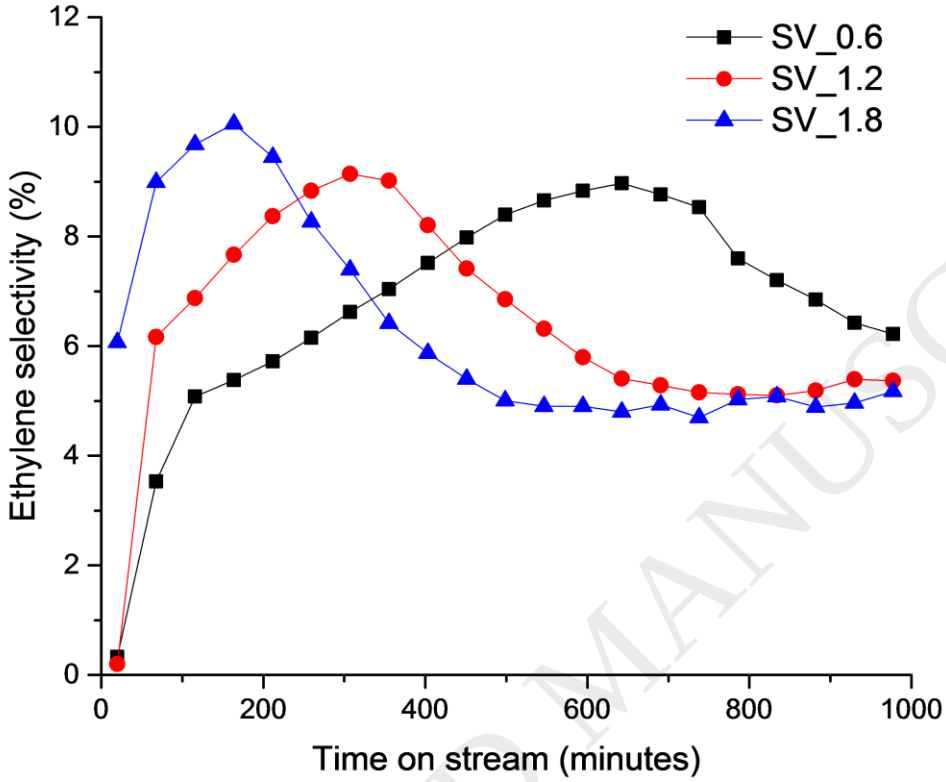

Figure 17: Effect of space velocity on benzene selectivity over 5% Mo/SZ catalyst (650 ^{o}C, 1 atm). SV has units of L.gcat^{-1}.hr^{-1}.

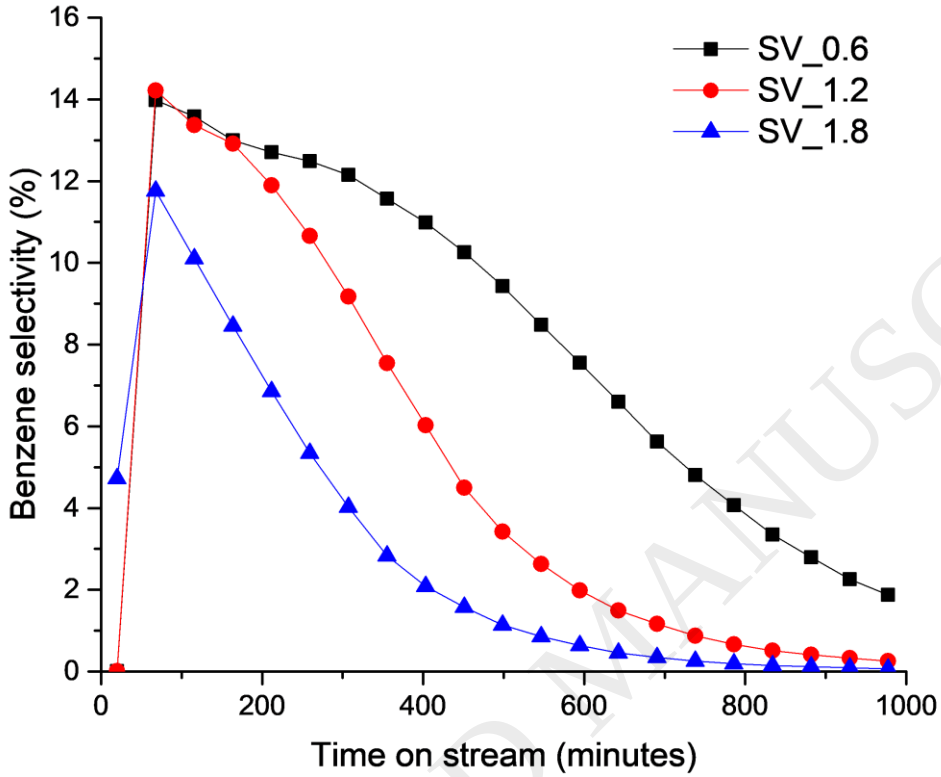

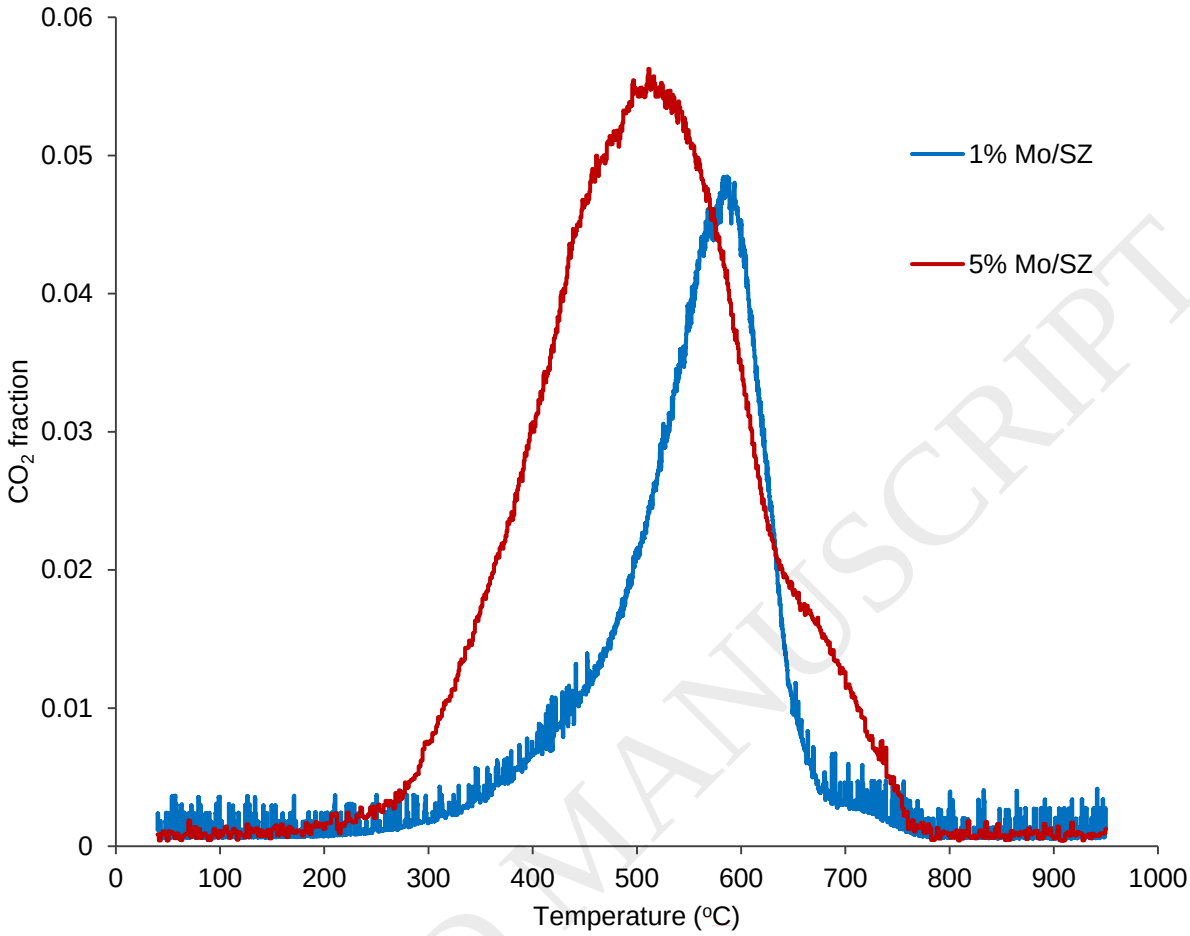

Figure 18: TPO profiles for the two spent catalysts (after DHA reaction for 16 hrs at 650 °C, 0.6 L.gcat^{-1}.hr^{-1}, 1 atm)

Figure 19: TPO profiles for the two spent catalysts (after DHA reaction for 16 hrs at 650 ^{o}C, 0.6 L.gcat^{-1}.hr^{-1}, 1 atm)

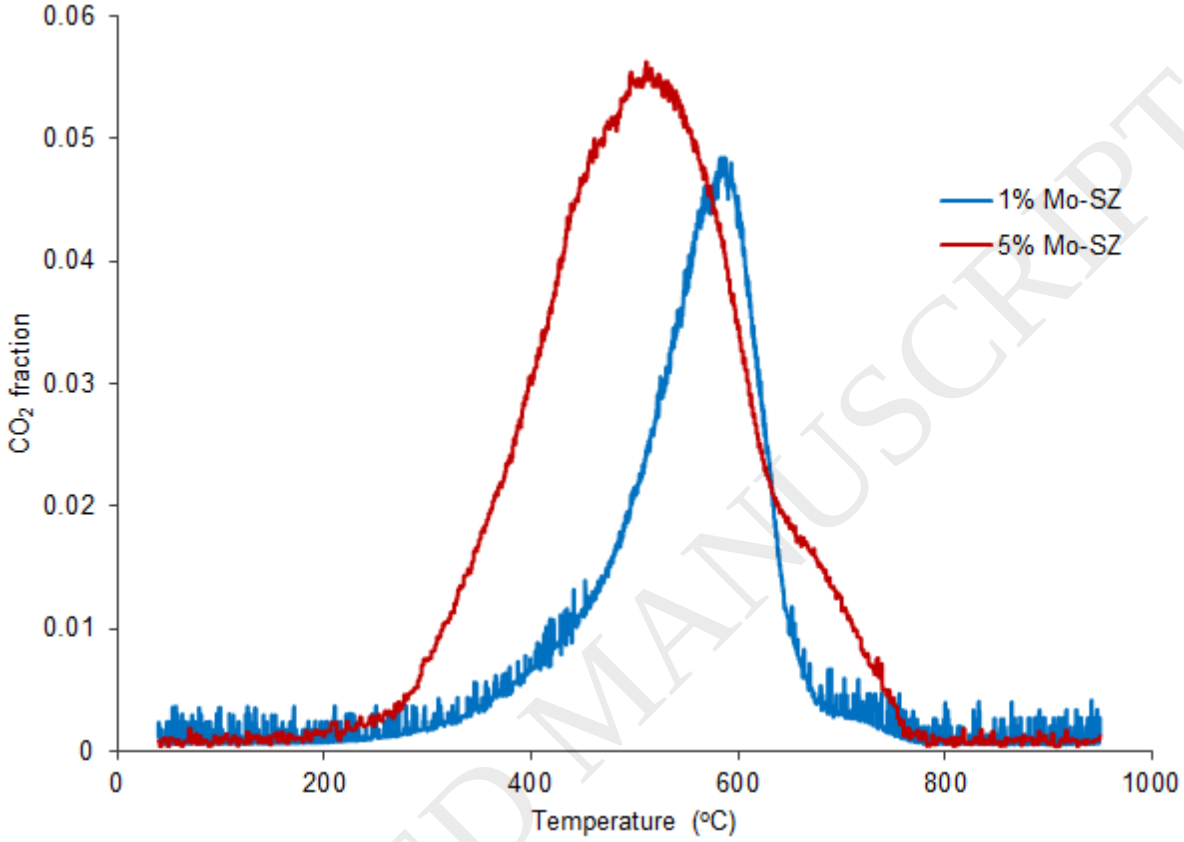

Table 1: Physico-chemical properties of Mo/SZ

Catalyst	Mo loading, % (intended)	Mo loading, wt% (ICP)	Mo loading, wt% (EDS)	S loading, wt% (ICP)	BET Surface Area (m^2/g)
SZ	0	0	0	3.5	84
1% Mo/SZ	1	0.84	1.6	2.99	87
5% Mo/SZ	5	3.92	4.5	1.95	76

Table 2: Effect of temperature on CH_4 DHA over 5% Mo/SZ catalyst (1 atm, 0.6 $L.gcat^{-1}hr^{-1}$). Results are at 2 hrs into the reaction.

Temperature (°C)	CH_4 conversion (%)	Aromatics selectivity (%)	Aliphatics selectivity (%)	Naphthalene + coke selectivity (%)
600	5.43	16.0	16.3	67.6
650	17.0	14.0	9.4	76.6
700	20.2	11.0	10.7	78.2

Table 3: Comparison of reaction performance with literature

Catalyst	Mo content (wt%)	Temperature (°C)	Space velocity ($L.gcat^{-1}.hr^{-1}$)	Max. Benzene yield (%)	Reference
Mo/H-ZSM-5	6	675	1.5	3	[63]
MoH-ZSM-5	6	700	1.5	6	[63]
Mo/H-ZSM-5	5	700	1.5	6	[60]
Mo/H-ZSM-5	5	700	0.8[a]	11	[31]
Mo/H-Mordenite	5	700	2.0[a]	0.5	[34]
Mo/H-SSZ-13	5	700	2.0[a]	negligible	[34]
Mo/SZ	5	650	1.2	1.8	Current work
Mo/SZ	5	700	0.6	3	Current work

[a] Units of hr^{-1}

Table 4: Quantification of coke using TPO (after ~ 16 hrs on stream)

Catalyst	Amount of coke deposited (mmol/gcat)
1% Mo/SZ	5.80
5% Mo/SZ	10.5